Different dynamics of a periodic mass-in-mass nonlinear chain during a single mode excitation

Jean Flosi, Claude-Henri Lamarque, Alireza Ture Savadkoohi

DIFFERENT DYNAMICS OF A PERIODIC MASS-IN-MASS NONLINEAR CHAIN DURING A SINGLE MODE EXCITATION

J. Flosi*
Univ Lyon, ENTPE, Ecole Centrale de Lyon, CNRS, LTDS, UMR5513
Rue Maurice Audin F-69518 Vaulx-en-Velin Cedex, France
jean.flosi@entpe.fr

C.-H. Lamarque
Univ Lyon, ENTPE, Ecole Centrale de Lyon, CNRS, LTDS, UMR5513
Rue Maurice Audin F-69518 Vaulx-en-Velin Cedex, France
lamarque@entpe.fr

A. Ture Savadkoohi
Univ Lyon, ENTPE, Ecole Centrale de Lyon, CNRS, LTDS, UMR5513
Rue Maurice Audin F-69518 Vaulx-en-Velin Cedex, France
alireza.turesavadkoohi@entpe.fr

ABSTRACT

The multiple scale dynamics of a periodic chain composed of nonlinear mass-in-mass cells is studied. Based on a continuous approach of the one-dimensional chain, dispersion equation is obtained which provides the general form of solutions of the linearized system. Taking into account a single harmonic of the chain around a 1:1 resonance with a targeted mode, fast dynamics of the system leads to the detection of the slow invariant manifold and its stability borders. Slow dynamics permits to predict singularities and equilibrium points leading to frequency responses. The developments predict periodic and non-periodic responses and permit to tune parameters of the chain for the aim of localization of vibrating energy and design of periodic or non-periodic responses.

***K*eywords** nonlinear metamaterials · mass-in-mass cells · periodic/non-periodic system · multiple scale method

1 Introduction

Metamaterials can present unusual characteristics due to their special designs. There is no exact known date of the first developed metamaterial, but it seems that the first works were led in the electromagnetic field, where Veselago (1) was able to predict negative electric permittivity and magnetic permeability. Other developments in the magnetic field (2) have been carried out and similar ideas have been conducted in optical and mechanical fields. For instance, special design allows to obtain desired Poisson ratio via using (for example) origami based structures. Bertoldi et al. (3) designed several types of mechanical metamaterials via exploitation of instabilities in mechanical systems. Topologies are endowed to change physical properties of the material. Mechanical metamaterials have also applications in the vibro-acoustic field as passive, active or adaptive materials (4). Negative indices such as negative effective mass induce bandgaps (5) in the vibro-acoustic fied. One of techniques for designing vibro-acoustic metamaterials is to assemble cells with special characteristics. Different types of linear cells have been investigated, for instance cells in a chain with translational and rotational motions for creation of negative effective mass and stiffness (6). Huang et al. (7) studied membranes and plate-types mass-in-mass system to tune the effective density. Meanwhile, nonlinearities are introduced in systems for exploiting their advantageous with respect to the linear systems. Different methods such as Harmonic

*Corresponding author

Balance (8) or Normal Form (9; 10) permits to determine the frequency response of the nonlinear systems. Lazarov et al. (11) used nonlinear chain (pure cubic and duffing type) for controlling low-frequency wave transmissions by high-frequency standing waves in some part of the chain. Some applications of such kinds of vibro-acoustic chains are reported in (12; 13; 14; 15). One of the special types of architected meta-cells is the mass-in-mass system (16). Nonlinear version of such system with inclusion of linear and cubic restoring forces is studied by Cveticanin et al. (17). Based on the notion of negative effective mass, they managed to obtain bandgaps for the unit sub-system under particular forcing. The influence of the number of inclusions of inner-masses is studied by Rodrigues et al. (18). A chain of nonlinear mass-in-mass cells wit a special type of nonlinearity under particular excitation has been studied by Cveticanin et al. (19). Romeo and Rega (20) studied free wave propagation in a chain of oscillators grounded nonlinearly using nonlinear maps leading to determination of pass and stop band regions of the chain. Using complexification (21) and multiple scales methods (22), one can determine fast and slow system dynamics (23; 24), and also periodic and non-periodic system responses (25; 26). They can be extended to multi-degrees of freedom systems such as a chain of nonlinear oscillators (27). Manevitch et al. (28) investigated on a semi infinite chain presenting standing waves and energy transfer between nonlinear particles. The infinite cubic nonlinear chain for general forcing was studied by Lazarov et al. (29). Considering first and third harmonics of the system, they deduced bandgaps from the dispersion equation of the chain. Vakakis et al. (30) investigated on the forced infinite undamped chain of nonlinear oscillators by taking a continuous approximation of the system leading to particular motions of the chain depending on the forcing. Bacigalupo et al. (31) performed an optimal design of lattice metamaterials. Other similar works on infinite chains are articulated in (32; 33). These kinds of systems become achievable using new three-dimensional (3D) printing technologies (34; 35).

In this paper, we aim to consider a L-periodic discrete chain of nonlinear oscillators and we apply a continuous approach. The study is taking into account a mono-harmonic response in accordance with the excitation, meaning that we suppose that there is no modal interactions in the chain and that forcing frequency is closed to a natural frequency of the chain. The organization of the paper is as it follows: In Sec.2, the chain under consideration is presented and some primary treatments on the discrete governing equations are carried out, leading to obtaining the continuous form of system equations. Determination of modal characteristics of the continuous chain, complexification and detection of fast and slow dynamics of the non-projected system are illustrated in Sec.3. Analytical results are compared to numerical simulations in Sec.4. The conclusions of the paper are presented in Sec.5. In Appendices A and B, the projected system of equations on one of its modes in continuous and discrete domains are presented, treated and discussed, respectively.

2 The system and its primary treatments

2.1 Discrete form of governing system equations

In this study, a periodic mass-in-mass chain with a period of L cells presented in Fig.1, is considered. Each cell of the chain is composed of a principal and a secondary mass. For the j^{th} cell, $j = 1, ..., L$, u_j and v_j are respectively the displacements of the principal masses m_1^j and inner masses m_2^j. These masses are linked by a cubic stiffness k_3 and a linear damping c_2. The cell number j is linearly linked to its neighbor cells number $j-1$ and $j+1$ with a linear stiffness k_1 and linear damping c_1. Each cell is at a distance Δx at rest from its neighbor cells. Because of periodicity, the cells number 1 and L are neighbors, meaning that the principal mass of the cell 1 is linked to the principal mass of the cell L with a stiffness k_1 and linear damping c_1. Governing system equations are:

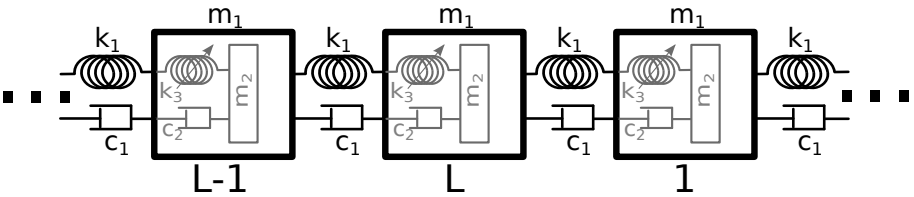

Figure 1: The considered discrete system around the cell $j = L$. At rest position, the distance between two neighbor cells is Δx.

$$\begin{cases} m_1\frac{d^2u_1}{dt^2} + k_1(2u_1 - u_L - u_2) + k_3(u_1 - v_1)^3 + c_1(2\frac{du_1}{dt} - \frac{du_L}{dt} - \frac{du_2}{dt}) \\ +c_2(\frac{du_1}{dt} - \frac{dv_1}{dt}) = F_1\sin(\Omega t) \\ m_1\frac{d^2u_j}{dt^2} + k_1(2u_j - u_{j-1} - u_{j+1}) + k_3(u_j - v_j)^3 + c_1(2\frac{du_j}{dt} - \frac{du_{j-1}}{dt} - \frac{du_{j+1}}{dt}) \\ +c_2(\frac{du_j}{dt} - \frac{dv_j}{dt}) = F_j\sin(\Omega t) \qquad \text{for } j = 2, ..., L-1 \\ m_1\frac{d^2u_L}{dt^2} + k_1(2u_L - u_{L-1} - u_1) + k_3(u_L - v_L)^3 + c_1(2\frac{du_L}{dt} - \frac{du_{L-1}}{dt} - \frac{du_1}{dt}) \\ +c_2(\frac{du_L}{dt} - \frac{dv_L}{dt}) = F_L\sin(\Omega t) \\ m_2\frac{d^2v_j}{dt^2} + k_3(v_j - u_j)^3 + c_2(\frac{dv_j}{dt} - \frac{du_j}{dt}) = 0 \qquad \text{for } j = 1, ..., L \end{cases} \tag{1}$$

For further developments, the complexified form of system equations (21), will be truncated via a Galerkin method (27), then the multiple scale method (22) will be used to detect different system dynamics.
Let us set ε as the perturbation parameter where $0 < \varepsilon = \frac{m_2}{m_1} \ll 1$. We normalize the system using the new temporal variable $\tau = \omega t = \sqrt{\frac{k_1}{m_1}}t$. Let us introduce following parameters: $\varepsilon\Lambda = \frac{k_3}{k_1}$, $\varepsilon\chi_1 = \frac{c_1}{\sqrt{k_1 m_1}}$, $\varepsilon\chi_2 = \frac{c_2}{\sqrt{k_1 m_1}}$, $\varepsilon f_j = \frac{F_j}{k_1}$ and $\nu = \frac{\Omega}{\omega}$. Final discrete expression of the governing Eq.1 is:

$$\begin{cases} \frac{d^2u_j}{d\tau^2} + (2u_j - u_{j-1} - u_{j+1}) + \varepsilon\Lambda(u_j - v_j)^3 \\ +\varepsilon\chi_1(2\frac{du_j}{d\tau} - \frac{du_{j-1}}{d\tau} - \frac{du_{j+1}}{d\tau}) + \varepsilon\chi_2(\frac{du_j}{d\tau} - \frac{dv_j}{d\tau}) = \varepsilon f_j\sin(\nu\tau) \\ \text{for } j = 2, ..., L-1 \\ \frac{d^2u_1}{d\tau^2} + (2u_1 - u_L - u_2) + \varepsilon\Lambda(u_1 - v_1)^3 \\ +\varepsilon\chi_1(2\frac{du_1}{d\tau} - \frac{du_L}{d\tau} - \frac{du_2}{d\tau}) + \varepsilon\chi_2(\frac{du_1}{d\tau} - \frac{dv_1}{d\tau}) = \varepsilon f_1\sin(\nu\tau) \\ \frac{d^2u_L}{d\tau^2} + (2u_L - u_{L-1} - u_1) + \varepsilon\Lambda(u_L - v_L)^3 \\ +\varepsilon\chi_1(2\frac{du_L}{d\tau} - \frac{du_{L-1}}{d\tau} - \frac{du_1}{d\tau}) + \varepsilon\chi_2(\frac{du_L}{d\tau} - \frac{dv_L}{d\tau}) = \varepsilon f_L\sin(\nu\tau) \\ \varepsilon\frac{d^2v_j}{d\tau^2} + \varepsilon\Lambda(v_j - u_j)^3 + \varepsilon\chi_2(\frac{dv_j}{d\tau} - \frac{du_j}{d\tau}) = 0 \qquad \text{for } j = 1, ..., L \end{cases} \tag{2}$$

2.2 Continuous form of governing system equations

We are proposing a continuous approach for detection of different behaviors of the periodic chain. Let us define the position of a cell with the spatial coordinate X: the position of the j^{th} cell verifies $X = (j-1)\Delta x$, or $X = x\Delta x$. We choose to use the normalized coordinate, as $x = \frac{X}{\Delta x}$. The continuous displacement functions are defined as:

$$\begin{cases} u(x,\tau) = u(x = j-1, \tau), & x \in [0, L], \quad j = 1, ..., L+1 \\ v(x,\tau) = v(x = j-1, \tau), & x \in [0, L], \quad j = 1, ..., L+1 \end{cases} \tag{3}$$

Displacements can now be decomposed using Taylor series. In this way, $u(x = j-1, \tau)$ and $u(x = j+1, \tau)$ are expressed as:

$$\begin{cases} u(j-1,\tau) = u(j,\tau) - \Delta x \dfrac{\partial u}{\partial X}(j,\tau) + \dfrac{1}{2!}\Delta x^2 \dfrac{\partial^2 u}{\partial X^2}(j,\tau) + O(\Delta x^3) \\ = u(j,\tau) - \dfrac{\partial u}{\partial x}(j,\tau) + \dfrac{1}{2}\dfrac{\partial^2 u}{\partial x^2}(j,\tau) + O(\Delta x^3) \\ u(j+1,\tau) = u(j,\tau) + \Delta x \dfrac{\partial u}{\partial X}(j,\tau) + \dfrac{1}{2!}\Delta x^2 \dfrac{\partial^2 u}{\partial X^2}(j,\tau) + O(\Delta x^3) \\ = u(j,\tau) + \dfrac{\partial u}{\partial x}(j,\tau) + \dfrac{1}{2}\dfrac{\partial^2 u}{\partial x^2}(j,\tau) + O(\Delta x^3) \end{cases} \tag{4}$$

With the introduction of continuous variables, we can adapt dynamical expressions in Eq.2. Neglecting $O(\Delta x^3)$ in Eq.4, following continuous spatio-temporal system is obtained:

$$\begin{cases} \dfrac{\partial^2 u}{\partial \tau^2} - \dfrac{\partial^2 u}{\partial x^2} + \varepsilon\Lambda(u-v)^3 - \varepsilon\chi_1(\dfrac{\partial}{\partial\tau}\dfrac{\partial^2 u}{\partial x^2}) + \varepsilon\chi_2(\dfrac{\partial u}{\partial\tau} - \dfrac{\partial v}{\partial\tau}) = \varepsilon f(x)\sin(\nu\tau) \\ \varepsilon\dfrac{\partial^2 v}{\partial\tau^2} + \varepsilon\Lambda(v-u)^3 + \varepsilon\chi_2(\dfrac{\partial v}{\partial\tau} - \dfrac{\partial u}{\partial\tau}) = 0 \end{cases} \tag{5}$$

We introduce following continuous variables:

$$\begin{cases} U(x,t) = u(x,t) \\ V(x,t) = u(x,t) - v(x,t) \end{cases} \tag{6}$$

Equation 5 reads:

$$\begin{cases} \dfrac{\partial^2 U}{\partial\tau^2}(x,\tau) - \dfrac{\partial^2 U}{\partial x^2}(x,\tau) + \varepsilon\Lambda V^3(x,\tau) - \varepsilon\chi_1\dfrac{\partial}{\partial\tau}\dfrac{\partial^2 U}{\partial x^2}(x,\tau) + \varepsilon\chi_2\dfrac{\partial V}{\partial\tau}(x,\tau) \\ = \varepsilon f(x)\sin(\nu\tau) \\ \dfrac{\partial^2(U-V)}{d\tau^2}(x,\tau) - \Lambda V^3(x,\tau) - \chi_2\dfrac{\partial V}{\partial\tau}(x,\tau) = 0 \end{cases} \tag{7}$$

Moreover, we suppose a periodic chain via imposing following conditions:

$$\begin{cases} U(x,\tau) = U(x+L,\tau) \\ V(x,\tau) = V(x+L,\tau) \\ \frac{\partial U}{\partial x}(x,\tau) = \frac{\partial U}{\partial x}(x+L,\tau) \\ \frac{\partial V}{\partial x}(x,\tau) = \frac{\partial V}{\partial x}(x+L,\tau) \end{cases} \tag{8}$$

We now have the final continuous expression of the system and we can begin the multiple scale study in the following Sec.3.

3 Time multiple scale responses of the system

Applying the multiple scale method (22), time is decomposed in fast time (τ_0) and slow times ($\tau_k, k = 1, 2, ...$) linked together by the mass ratio ε:

$$\tau_0 = \tau \qquad \text{and} \qquad \tau_k = \varepsilon^k\tau, \qquad k = 1, ... \tag{9}$$

and redefining derivation operator:

$$\frac{\partial}{\partial\tau} = \frac{\partial}{\partial\tau_0} + \varepsilon\frac{\partial}{\partial\tau_1} + ... \tag{10}$$

We use complex variables of Manevitch (21) in the domain of the adimensional angular frequency ν of the external excitation. We define:

$$\begin{cases} \phi(x,\tau)e^{i\nu\tau} = \dfrac{\partial U}{\partial\tau}(x,\tau) + i\nu U(x,\tau) \\ \psi(x,\tau)e^{i\nu\tau} = \dfrac{\partial V}{\partial\tau}(x,\tau) + i\nu V(x,\tau) \end{cases} \tag{11}$$

with $i^2 = -1$. A Galerkin technique is used to pick only the j^{th} harmonic of a function $s(\tau)$. This is carried out via (27):

$$\frac{\nu}{2\pi}\int_0^{\frac{2\pi}{\nu}} s(\tau)e^{-ij\nu\tau}d\tau \tag{12}$$

After the introduction of complex variables and application of Eq.12 in Eq.7, the following system is obtained:

$$\begin{cases} \left(\dfrac{\partial\phi}{\partial\tau}(x,\tau) + i\nu\phi(x,\tau)\right) - \dfrac{1}{i\nu}\dfrac{\partial^2\phi}{\partial x^2}(x,\tau) - \varepsilon\dfrac{3i\Lambda}{4\nu^3}\psi|\psi|^2(x,\tau) \\ -\varepsilon\chi_1\frac{\partial^2\phi}{\partial x^2}(x,\tau) + \varepsilon\chi_2\psi(x,\tau) = -i\varepsilon f(x) \\ \left(\dfrac{\partial(\phi-\psi)}{\partial\tau}(x,\tau) + i\nu(\phi-\psi)(x,\tau)\right) + \dfrac{3i\Lambda}{4\nu^3}\psi|\psi|^2(x,\tau) - \chi_2\psi(x,\tau) = 0 \end{cases} \tag{13}$$

3.1 Dispersion relation

For the evaluation of modes of the continuous system, we come back to the physical expression of the system and we consider the linearized form of Eq.7 by withdrawing forcing, cubic interactions and damping. It reads:

$$\begin{cases} \dfrac{\partial^2 U_l}{\partial\tau^2}(x,\tau) - \dfrac{\partial^2 U_l}{\partial x^2}(x,\tau) = 0 \\ \dfrac{\partial^2(U_l - V_l)}{\partial\tau^2}(x,\tau) = 0 \end{cases} \tag{14}$$

In this case, U_l and V_l are periodic solutions and can be decomposed as:

$$\begin{cases} U_l(x,\tau) = U_l(x)e^{i\gamma\tau} \\ V_l(x,\tau) = V_l(x)e^{i\gamma\tau} \end{cases} \tag{15}$$

The first equation of Eq.14 becomes:

$$\gamma^2 U_l(x) + \frac{\partial^2 U_l}{\partial x^2}(x) = 0 \tag{16}$$

with $\gamma \in \mathbb{R}$. Solutions of this equation can be expressed as:

$$U_l(x) = A\cos(\gamma x) + B\sin(\gamma x) \qquad \text{with A,B} \in \mathbb{R}^2 \tag{17}$$

In order to determine the unknowns of Eq.17, we use boundary conditions of the periodic chain defined in Eq.8 and applied for $x = 0$:

$$\begin{cases} U_l(0,\tau) = U_l(L,\tau) \\ \dfrac{\partial U_l}{\partial x}(0,\tau) = \dfrac{\partial U_l}{\partial x}(L,\tau) \end{cases} \tag{18}$$

Injecting Eq.17 in Eq.18, the following system is obtained:

$$\underbrace{\begin{pmatrix} 1-\cos(\gamma L) & -\sin(\gamma L) \\ \sin(\gamma L) & 1-\cos(\gamma L) \end{pmatrix}}_{\mathscr{A}} \begin{pmatrix} A \\ B \end{pmatrix} = 0 \tag{19}$$

The non-trivial solution of Eq.19 imposes that:

$$\begin{array}{l} \det(\mathscr{A}) = 0 \implies 1-\cos(\gamma L) = 0 \\ \text{i.e.} \quad \gamma = \omega_k = \frac{2k\pi}{L} = k\omega_1 \quad \text{for } k \in \mathbb{N}, \quad \omega_1 = \frac{2\pi}{L} \end{array} \tag{20}$$

Then, general expression of $U_l(x)$ reads:

$$U_l(x,\tau) = \sum_{k=0}^{\infty}\left(A_k\cos(\omega_k x) + B_k\sin(\omega_k x)\right)e^{i\omega_k\tau} = \sum_{k=0}^{\infty}\tilde{\rho}_k\cos(\omega_k x + \Theta_k)e^{i\omega_k\tau} \tag{21}$$

with:

$$\begin{cases} \tilde{\rho}_k = \sqrt{A_k^2 + B_k^2} \\ \Theta_k = -\tan^{-1}(\frac{B_k}{A_k}) \end{cases} \tag{22}$$

In this study, we suppose that a single mode of the system, namely k^{th} mode, is responding. So, ignoring the rigid body motion (by setting $A_0 = B_0 = 0$), we set:

$$U_l(x,\tau) = \tilde{\rho}_k \cos(\omega_k x + \Theta_k) e^{i\omega_k \tau} \tag{23}$$

We are interested to look at system behaviors around the frequency ω_k of excitation. Then, in Eq.13, we set $\nu = \omega_k + \sigma\varepsilon$. The system becomes:

$$\begin{cases} \left(\frac{\partial\phi}{\partial\tau}(x,\tau) + i(\omega_k + \sigma\epsilon)\phi(x,\tau)\right) + \frac{\omega_k^2}{i(\omega_k+\sigma\epsilon)}\phi(x,\tau) \\ -\varepsilon\frac{3i\Lambda}{4(\omega_k+\sigma\varepsilon)^3}\psi|\psi|^2(x,\tau) + \varepsilon\chi_1\omega_k^2\phi(x,\tau) + \varepsilon\chi_2\psi(x,\tau) = -i\varepsilon f(x,\tau) \\ \left(\frac{\partial(\phi-\psi)}{\partial\tau}(x,\tau) + i(\omega_k + \sigma\varepsilon)(\phi-\psi)(x,\tau)\right) + \frac{3i\Lambda}{4(\omega_k+\sigma\varepsilon)^3}\psi|\psi|^2(x,\tau) \\ -\chi_2\psi(x,\tau) = 0 \end{cases} \tag{24}$$

i.e.:

$$\begin{cases} \left(\frac{\partial\phi}{\partial\tau_0}(x,\tau) + \varepsilon\frac{\partial\phi}{\partial\tau_1}(x,\tau) + 2i\sigma\epsilon\phi(x,\tau)\right) - \varepsilon\frac{3i\Lambda}{4\omega_k^3}\psi|\psi|^2(x,\tau) \\ +\varepsilon\chi_1\omega_k^2\phi(x,\tau) + \varepsilon\chi_2\psi(x,\tau) = -i\varepsilon f(x,\tau) + O(\varepsilon^2) \\ \left(\frac{\partial(\phi-\psi)}{\partial\tau_0}(x,\tau) + i\omega_k(\phi-\psi)(x,\tau)\right) + \frac{3i\Lambda}{4\omega_k^3}\psi|\psi|^2(x,\tau) - \chi_2\psi(x,\tau) = O(\varepsilon) \end{cases} \tag{25}$$

Because of the precedent identification of $U_l(x)$ (Eq.21, 23), we can deduce the general expression of U for the k^{th} mode as:

$$U(x,\tau) = (A_k\cos(\omega_k x) + B_k\sin(\omega_k x))\, G(\tau) e^{i\nu\tau} = \rho_k(\tau)\cos(\omega_k x + \Theta_k) \tag{26}$$

G being the consequence of damping and cubic terms in Eq.7. We admit that the inner masses have the same distribution of displacement along the chain and therefore $V(x,\tau)$ has a similar general expression to $U(x,\tau)$.

We can apply the same general form of expression to ϕ and ψ as Eq.26. General expression of ϕ and ψ are:

$$\begin{cases} \phi(x,\tau) = \rho_1(\tau)\cos(\omega_k x + \Theta_k) e^{i\theta_1(\tau)} = \tilde{N}_1(x,\tau) e^{i\theta_1(\tau)} \\ \psi(x,\tau) = \rho_2(\tau)\cos(\omega_k x + \Theta_k) e^{i\theta_2(\tau)} = \tilde{N}_2(x,\tau) e^{i\theta_2(\tau)} \end{cases} \tag{27}$$

In this case, the expressions of modes are clarified, and oscillations frequency is equal to modal frequency of the system. In the next section, a multiple scale method is exploited to detect different system dynamics.

3.2 Fast dynamics of the system

3.2.1 Slow Invariant Manifold

Equation 25 at the order ε^0 reads:

$$\begin{cases} \frac{\partial\phi}{\partial\tau_0} = 0 \\ \frac{\partial\phi}{\partial\tau_0} - \frac{\partial\psi}{\partial\tau_0} + \mathcal{H}(\phi,\phi^*,\psi,\psi^*) = 0 \end{cases} \tag{28}$$

with

$$\mathcal{H}(\phi,\phi^*,\psi,\psi^*) = i\omega_k\phi - i\omega_k\psi + \frac{3i\Lambda}{4\omega_k^3}\psi|\psi|^2 - \chi_2\psi \tag{29}$$

The Slow Invariant Manifold (SIM) of the system is obtained by looking for fixed points of the system. They are verifying first relation of Eq.28 and the following condition:

$$\lim_{\tau_0\to+\infty}\frac{\partial\psi}{\partial\tau_0} = 0 \tag{30}$$

leading to $\mathcal{H}$=0 (see Eq.28). So, we can write:

$$\phi = \psi - \frac{i\chi_2}{\omega_k}\psi - \frac{3\Lambda}{4\omega_k^4}\psi^2\psi^* \tag{31}$$

and finally introduce polar coordinates for complex variables defined in Eq.27. We obtain:

$$\begin{aligned}&\mathcal{H}(\tilde{N}_1,\theta_1,\tilde{N}_2,\theta 2)=i\tilde{N}_1(x,\tau_1,...)e^{i(\theta_1-\theta_2)}+\frac{3i\Lambda}{4\omega_k^4}\tilde{N}_2^3(x,\tau_1,...)\\&-\tfrac{\chi_2}{\omega_k}\tilde{N}_2(x,\tau_1,...)-i\tilde{N}_2(x,\tau_1,...)=0\end{aligned}\tag{32}$$

where $\tilde{N}_1,\tilde{N}_2\in\mathbb{R}^2$ and $\theta_1,\theta_2\in\mathbb{R}^2$.
We set $N_1(x,\tau)=|\tilde{N}_1(x,\tau)|$ and $N_2(x,\tau)=|\tilde{N}_2(x,\tau)|$, $N_1,N_2\in\mathbb{R}_+^2$. Then, for all the spatial coordinates verifying $\cos(\omega_k x+\Theta_k)\neq 0$, we have:

$$N_1(x,\tau_1,\dots)=\sqrt{\left(N_2(x,\tau_1,\dots)-\tfrac{3\Lambda}{4\omega_k^4}N_2^3(x,\tau_1,\dots)\right)^2+\left(\tfrac{\chi_2}{\omega_k}N_2(x,\tau_1,\dots)\right)^2}\tag{33}$$

Otherwise, when x verifies $\cos(\omega_k x+\Theta_k)=0$, the solution of Eq.32 is
$N_1(x,\tau_1,\dots)=N_2(x,\tau_1,\dots)=0$.

We can observe that the expression of the SIM in Eq.33 does not directly depend on the position of the cell in the chain. However, the dependency on x appears when we use the developed expressions of $\tilde{N}_1(x,\tau)=\rho_1(\tau)\cos(\omega_k x+\Theta_k)$ and $\tilde{N}_2(x,\tau)=\rho_2(\tau)\cos(\omega_k x+\Theta_k)$ from Eq.27.
Due to damping term χ_2 between principal and inner masses, the only solution compatible with $N_1(x,\tau_1,\dots)=0$ is $N_2(x,\tau_1,\dots)=0$. However, when $\chi_2=0$, two solutions $N_2(x,\tau_1,\dots)=0$ and $N_2(x,\tau_1,\dots)=\frac{2\omega_k^2}{\sqrt{3\Lambda}}$ satisfy $N_1(x,\tau_1,\dots)=0$.
Detection of the SIM can be carried out after applying modal projection in the Eq.13. This work is presented in Appendix in Sec.5. The general geometry of the SIM is the same as the one defined in Eq.33.
In order to justify the continuous approach, we also provide a discrete approach of the system in Appendix. We compare results obtained via discrete and continuous approaches. The use of continuous approach provides similar results with the ones of the discrete approach, even when the chain is composed of a limited amount of cells.
In the next subsection, stability zones of the SIM are clarified.

3.2.2 Stable analysis of the SIM

In order to trace stability of the SIM, we linearly perturb the variable ψ as it follows:

$$\begin{cases}\psi\to\psi+\Delta\psi\\ \psi^*\to\psi^*+\Delta\psi^*\end{cases}\qquad\text{where }|\Delta\psi|\ll|\psi|\tag{34}$$

We don't perturb the function ϕ because ϕ is independent of the fast time scale τ_0 as it is shown in Eq.28 .
Therefore, Eq.29 reads:

$$\begin{cases}\frac{\partial(\psi+\Delta\psi)}{\partial\tau_0}=\mathcal{H}(\phi,\psi+\Delta\psi,\psi^*+\Delta\psi^*)\\ \frac{\partial(\psi^*+\Delta\psi^*)}{\partial\tau_0}=\mathcal{H}^*(\phi^*,\psi+\Delta\psi,\psi^*+\Delta\psi^*)\end{cases}\tag{35}$$

Eq.35 being written in a matrix form leads to the definition of the matrix $\mathscr{B}$:

$$\begin{pmatrix}\frac{\partial\Delta\psi}{\partial\tau_0}\\ \frac{\partial\Delta\psi^*}{\partial\tau_0}\end{pmatrix}=\underbrace{\begin{pmatrix}\frac{3i\Lambda\psi\psi^*}{2\omega_k^3}-\chi_2-i\omega_k & \frac{3i\Lambda\psi^2}{4\omega_k^3}\\ -\frac{3i\Lambda\psi^*\psi^*}{4\omega_k^3} & -\frac{3i\Lambda\psi\psi^*}{2\omega_k^3}-\chi_2+i\omega_k\end{pmatrix}}_{\mathscr{B}}\begin{pmatrix}\Delta\psi\\ \Delta\psi^*\end{pmatrix}\tag{36}$$

The characteristic polynomial of $\mathscr{B}$ is:

$$P(X)=X^2+2\chi_2X+\omega_k^2+\chi_2^2-\tfrac{3\Lambda}{\omega_k^2}\psi\psi^*+\tfrac{27\Lambda^2}{16\omega_k^6}\psi^2\psi^*\psi^*\tag{37}$$

Unstable zones of the SIM verify:

$$\omega_k^2+\chi_2^2-\tfrac{3\Lambda}{\omega_k^2}\psi\psi^*+\tfrac{27\Lambda^2}{16\omega_k^6}\psi^2\psi^*\psi^*<0\tag{38}$$

Therefore, the stability borders of the system verify:

$$\omega_k^2+\chi_2^2-\tfrac{3\Lambda}{\omega_k^2}\psi\psi^*+\tfrac{27\Lambda^2}{16\omega_k^6}\psi^2\psi^*\psi^*=0\tag{39}$$

Using polar coordinates from Eq.27, the roots of this fourth order in N_2 polynomial are:

$$\begin{cases} N_{21} = \dfrac{2}{3}\sqrt{\dfrac{2\omega_k^4 - \omega_k^3\sqrt{\omega_k^2 - 3\chi_2^2}}{\Lambda}} \\ N_{22} = \dfrac{2}{3}\sqrt{\dfrac{2\omega_k^4 + \omega_k^3\sqrt{\omega_k^2 - 3\chi_2^2}}{\Lambda}} \end{cases} \tag{40}$$

These values are real only if $\omega_k \geq \sqrt{3}\chi_2$. The SIM is unstable if N_2 verifies $N_{21} < N_2 < N_{22}$. In the next subsection, the behavior of the system at slow time scale is detected leading to detection of characteristic points of the system.

3.3 Slow dynamics

In this subsection, we are interested by the system behavior at slow time scale and we will detect characteristic points, which are singular or equilibrium points. This will help us to identify periodic or quasi-periodic regimes. We begin by considering the first equation in Eq.25 with forcing and we only consider the first order in ε:

$$\frac{\partial \phi}{\partial \tau_1}(x,\tau) + \mathcal{E}_1(\phi, \phi^*, \psi, \psi^*, \sigma) = 0 \tag{41}$$

with:

$$\begin{aligned} &\mathcal{E}_1(\phi, \phi^*, \psi, \psi^*, \sigma) = 2i\sigma\phi(x,\tau) - \tfrac{3i\Lambda}{4\omega_k^3}\psi|\psi|^2(x,\tau) + \chi_1\omega_k^2\phi(x,\tau) \\ &+\chi_2\psi(x,\tau) + if(x) \end{aligned} \tag{42}$$

The evolution of the SIM $\mathcal{H}(\phi, \phi^*, \psi, \psi^*)$ at τ_1 time scale, i.e. $\frac{\partial \mathcal{H}}{\partial \tau_1}$ and $\frac{\partial \mathcal{H}^*}{\partial \tau_1}$, is expressed as following:

$$\underbrace{\begin{pmatrix} \frac{\partial \mathcal{H}}{\partial \psi} & \frac{\partial \mathcal{H}}{\partial \psi^*} \\ \frac{\partial \mathcal{H}^*}{\partial \psi} & \frac{\partial \mathcal{H}^*}{\partial \psi^*} \end{pmatrix}}_{\mathscr{B}} \begin{pmatrix} \frac{\partial \psi}{\partial \tau_1} \\ \frac{\partial \psi^*}{\partial \tau_1} \end{pmatrix} = - \begin{pmatrix} \frac{\partial \mathcal{H}}{\partial \phi} & \frac{\partial \mathcal{H}}{\partial \phi^*} \\ \frac{\partial \mathcal{H}^*}{\partial \phi} & \frac{\partial \mathcal{H}^*}{\partial \phi^*} \end{pmatrix} \begin{pmatrix} \frac{\partial \phi}{\partial \tau_1} \\ \frac{\partial \phi^*}{\partial \tau_1} \end{pmatrix} \tag{43}$$

3.3.1 Singular points

Singular points are characteristics points verifying (36):

$$\begin{cases} \mathcal{H}(\phi, \phi^*\psi, \psi^*) = 0 \\ \mathcal{E}_1(\phi, \phi^*, \psi, \psi^*, \sigma) = 0 \\ \det(\mathscr{B}) = 0 \end{cases} \tag{44}$$

Application of conditions listed in Eq.44 in Eq.43 reads:

$$\begin{aligned} &\det(\mathscr{B}) = 0 \quad \text{with } \mathscr{B} = \begin{pmatrix} \frac{3i\Lambda\psi\psi^*}{2\omega_k^3} - \chi_2 - i\omega_k & \frac{3i\Lambda\psi^2}{4\omega_k^3} \\ -\frac{3i\Lambda\psi^*\psi^*}{4\omega_k^3} & -\frac{3i\Lambda\psi\psi^*}{2\omega_k^3} - \chi_2 + i\omega_k \end{pmatrix} \\ &\implies \frac{27\Lambda^2}{16\omega_k^6}\psi^2\psi^{*2} - \frac{3\Lambda}{\omega_k^2}\psi\psi^* + \chi_2^2 + \omega_k^2 = 0 \end{aligned} \tag{45}$$

and solutions are reported in Eq.40. Associated N_1 values are:

$$\begin{cases} N_{11} = \frac{2}{9}\sqrt{2}\sqrt{\omega_k\frac{\omega_k^3 + 9\omega_k\Lambda\chi_2^2 + (\omega_k^2 - 3\chi_2^2)\sqrt{\omega_k^2 - 3\chi_2^2}}{\Lambda}} \\ N_{12} = \dfrac{2}{9}\sqrt{2}\sqrt{\omega_k\dfrac{\omega_k^3 + 9\omega_k\Lambda\chi_2^2 - (\omega_k^2 - 3\chi_2^2)\sqrt{\omega_k^2 - 3\chi_2^2}}{\Lambda}} \end{cases} \text{ if } \omega_k \geq \sqrt{3}\chi_2 \tag{46}$$

The 2 singular point coordinates are (N_{21}, N_{11}) and (N_{22}, N_{12}).

3.3.2 Equilibrium points

Equilibrium points of the system verify:

$$\begin{cases} \mathcal{H}(\phi, \phi^*\psi, \psi^*) = 0 \\ \mathcal{E}_1(\phi, \phi^*, \psi, \psi^*, \sigma) = 0 \\ \det(\mathscr{B}) \neq 0 \end{cases} \tag{47}$$

We work on the function $\mathcal{E}_1(\phi, \phi^*, \psi, \psi^*, \sigma)$ defined in Eq.42 and we apply conditions listed in Eq.47. Injecting Eq.31 in Eq.42, we have the simplified relation:

$$\begin{array}{l} \mathcal{E}_1(\psi, \psi^*, \sigma) = \frac{\chi_1\left(-3\Lambda_k\psi^2\psi^* - 4i\chi_2\omega_k^3\psi + 4\omega_k^4\psi\right)}{4\omega_k^2} + \chi_2\psi + if(x) \\ + \frac{i\sigma\left(-3\Lambda\psi^2\psi^* - 4i\chi_2\omega_k^3\psi + 4\omega_k^4\psi\right)}{2\omega_k^3} - \frac{3i\Lambda\psi^2\psi^*}{4\omega_k^3} = 0 \end{array} \tag{48}$$

Once polar coordinates from Eq.27 are introduced, following cubic polynomial is obtained:

$$AX^3 + BX^2 + CX + D = 0 \tag{49}$$

with

$$\begin{cases} A = \frac{9\Lambda^2}{16\omega_k^8}(\omega_k^2 + 4\sigma\omega_k + 4\sigma^2 + \chi_1^2\omega^4) \\ B = -\frac{3\Lambda}{2\omega_k^4}(4\sigma^2 + 2\sigma\omega_k + \chi_1^2\omega_k^4) \\ C = 4\sigma^2 + 2\chi_1\chi_2\omega_k^2 + \chi_1^2\omega_k^4 + \frac{\chi_2^2(4\sigma^2 + 4\sigma\omega_k + \omega_k^2 + \chi_1^2\omega_k^4)}{\omega_k^2} \\ D = -f^2 \\ X = \tilde{N}_2^2 \end{cases} \tag{50}$$

For sweeping of σ, Eq.49 can be solved by Cardan's method to obtain corresponding N_2. Then, N_1 can be evaluated via Eq.33. Backbone curves of the system are obtained by setting $f = 0$, $\chi_1 = 0$, and $\chi_2 = 0$ in Eq.49.

3.3.3 Some remarks on the design of the SIM

For designing the SIM, we aim to have a non-monotone curve and therefore to have two non-identical singularity amplitudes. From the determination of the amplitude of singular points, which coincide with stability borders, it's interesting to plot the evolution of these borders as function of $\frac{k}{L}$ directly linked to ω_k, as depicted on Fig.2.
When $\frac{k}{L} \ll 1$, the design requires very small values of physical parameters Λ and χ_2 in order to maintain the presence of unstable zone of the SIM. Otherwise, either should the number of cell of the chain be reduced or the frequency of the mode of excitation be high in order to increase $\frac{k}{L}$ (or ω_k). Unstable zone only appears when the condition in Eq.38 is verified, i.e. $\frac{k}{L} > \frac{\sqrt{3}}{2\pi}\chi_2$.

Plotting the evolution of borders of unstable zones in the N_2 and N_1 axis illustrates the fact that the unstable zone becomes larger with the increase of $\frac{k}{L}$. Going to higher modes, i.e. increasing ω_k, the unstable zone of the SIM becomes wider leading to wider interval of N_2 for presentation of possible non-periodic responses. As the number of the mode (k) increases, the distance between N_{11} and N_{12} increases as well, meaning a large interval of variations of N_1 during quasi-periodic responses corresponding to repeated bifurcations.

The analytical study has been conducted and results will be compared to numerical simulation in the next Sec.4.

4 Numerical results

4.1 Numerical process

In this section, analytical developments are compared to results obtained from direct numerical integration of Eq.2. In the whole paper, we name the latter as "numerical results". Therefore, we are confronting predictions obtained from the continuous system to those obtained from numerical integration of the initial discrete system. This is done using the "ode45" function of Matlab® which is based on the Runge Kutta scheme. In order to have precise results, the relative and absolute error tolerances are set to 10^{-13}. The control error relative to norm is also set to 10^{-13}. Different

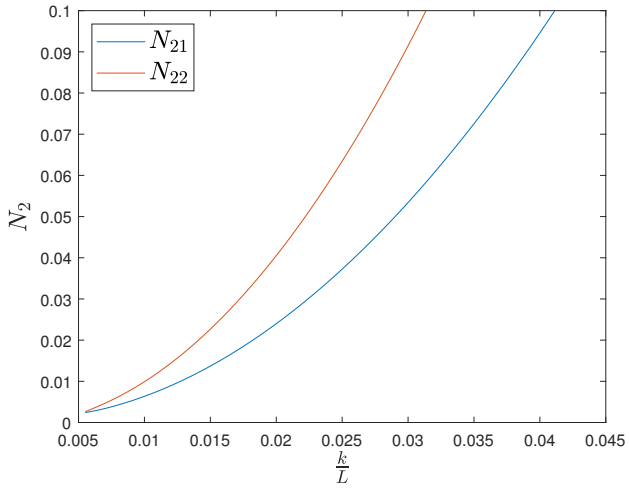

(a)

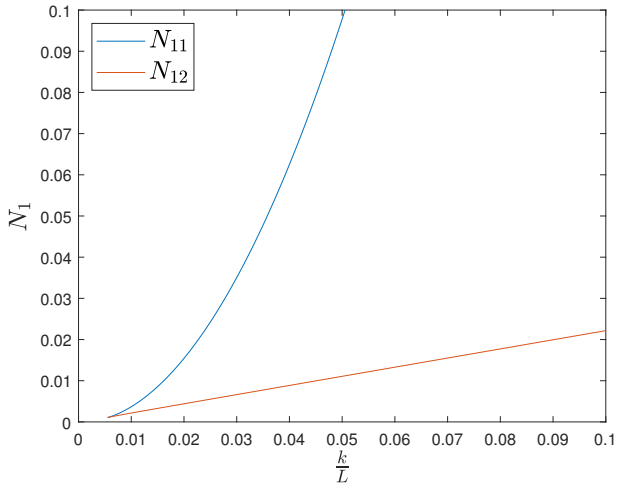

(b)

Figure 2: Evolution of amplitudes of singular points of the SIM with respect to $\frac{k}{L}$: (a) N_{21} and N_{22} (see Eq.40), (b) N_{11} and N_{12} (see Eq.46).

cases of initial conditions and forcing are investigated, but the initial speed and acceleration of masses are always set to zero. For non zero initial conditions of the free case, we suppose that $u_j(\tau = 0) = \tilde{\rho}\cos(\omega_k(j-1) + \Theta_i)$ and $v_j(\tau = 0) = 0$, $j = 1, \ldots, L$, meaning that the initial conditions follow general modal deformation of the chain which is defined in Eq.23. For the whole numerical results, we set $\Theta_k = \Theta_i$. The same pattern of distribution for the external excitation is applied i.e. $f(x, \tau) = f_0 \cos(\omega_k x + \Theta_f)\sin(\gamma\tau)$ meaning that $\Theta_k = \Theta_f$.

Table 1: Characteristics of the system for numerical verification

Configuration 1					Configuration 2					Configuration 3				
L	ε	χ_1	χ_2	Λ	L	ε	χ_1	χ_2	Λ	L	ε	χ_1	χ_2	Λ
10	0.001	0.1	0.02	0.2	100	0.001	0.1	0.02	0.2	100	0.01	0.1	0.02	0.2

The discrete system takes L cells in consideration constituted from a total number of $2L$ masses. The numerical integration returns $4L$ different values at each step of the time integration : $u_j(\tau)$ and $v_j(\tau)$, $j = 1, \ldots, L$ and their first derivatives $\dot{u}_j(\tau)$ and $\dot{v}_j(\tau)$, $j = 1, \ldots, L$. Complex variables of Manevitch are then computed as described by

Eq.6 and Eq.11. We keep the first harmonics of numerical results. The characteristics of the system are given in configuration 2 and 3 in Table 1.

4.2 Free responses of the system

The results are plotted in Fig.3 to Fig.6 for different cell positions and modes. On each of these figures, three results are presented for each chosen cell. The first one (a) presents the given initial displacement of the chain and marks with a red cross the position of the investigated cell of the discrete system. Time histories of $N_1(\tau)$ of the investigated cell are presented in (b) and confrontation between the SIM (green line) and results from numerical integration (red line) for the investigated cell are plotted in (c). Black '+' symbols stand for singular points and unstable zone is plotted in orange. Two cases of initial deformations ($k = 1$ and $k = 3$) are applied as $u_j(\tau = 0) = \tilde{\rho}\cos(\omega_k(j-1) + \Theta_k)$ and $v_j(\tau = 0) = 0$, $j = 1, \ldots, L$.
We can observe that due to the distribution of the initial deformation which follows the form of the mode along the chain, each cell has different initial energy and depending on this energy, it can face bifurcation(s) due to the existence of singularities. We can see that final state of the system is $u_j(\tau) = v_j(\tau) = 0$ when $\tau \to \infty$ as the damped system is free. Analytical and numerical results are in good agreement. The difference between the SIM and numerical results could have different reasons. For example, in applying complexes variables of Manevitch (Eq.27), we kept the first harmonics while one can take the effects of higher harmonics as well, for instance the third harmonics as Bitar et al. (36) did in their works. Moreover, it can be also due to internal resonances which are omitted in this paper.

4.3 Forced responses of the system

Here, we present some results corresponding to periodic and non-periodic regimes. Different forcing terms are considered. Figures 7-15 correspond to a periodic response of the chain due to the excitation with the frequency around the first mode of the system, i.e. ω_1. Figures 16-20 present quasi-periodic response of the system under external excitation with the frequency around the third mode, i.e. ω_3. Globally speaking, these results can be presented for any modes.
In the first case, the system is with zero initial conditions and under excitation with the amplitude of $f_j = 0.03\cos(\omega_1(j-1))$ and frequency $\nu = 0.064$. Parameters of the system are listed in configuration number 2 in Table 1. As some representative examples, frequency response curves for cells 1, 21 and 27 are presented respectively in Fig.7a,7c and 8a with the backbones curves plotted in black. Predicted equilibrium points for the given frequency ν are compared to numerical results in Fig.7b,7d and 8b. Figures 9-11 show the SIM (in green) accompanied by results obtained from direct numerical integration for the three considered cells. Singular points are represented by black '+' symbols and unstable zone is plotted in orange. In Fig.9 and 10 associated to cells 1 and 21, we can see repeated bifurcations during the transient response of the system before it reaches to the periodic regime.
Figure 12 and 13 show 3D and 2D views of analytical predictions of equilibrium points of the continuous system (green line) along the chain of 100 cells ($x \in [0; 99]$) for the system with $\nu = 0.064$. Equilibrium points obtained from numerical results, when $\tau \to \infty$ ($\tau > 9.988 \times 10^5$) are added to Fig.13 in black '+' symbols. Unstable zones are plotted in orange. This result shows that for this spatial case ($k = 1$), there are at least two cells where the physical displacement of the principal mass is very close to 0. From Fig.13, it is seen that there is good agreement between predicted N_1 and corresponding numerical results while the discrepancy between analytical and numerical N_2 increases in some zones of the chain. The possible reasons for these differences are explained in Section 4.2. The chain is also separated in two groups with a phase lag of π which can be verified in Fig.14 presenting time histories of the physical variables $u_j(\tau)$ for the mode 1 ($k = 1$) along the chain during periodic behavior when $\tau \to \infty$ ($\tau > 9.988 \times 10^5$). The similar representation for $v_j(\tau)$ is illustrated in Fig.15 during transient response. As seen before in Figs.9-11, some cells present repeated bifurcations before having periodic response associated to periodic equilibrium points predicted in Fig.12 and 13.

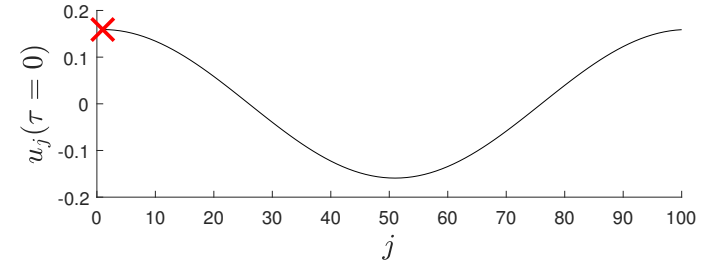

(a)

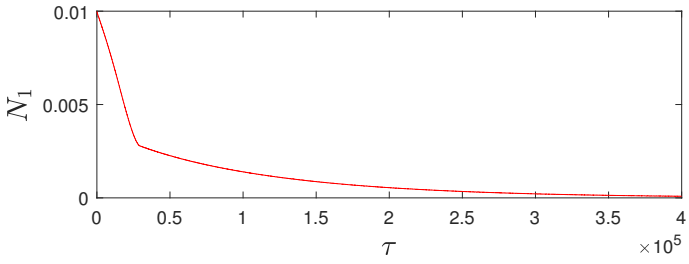

(b)

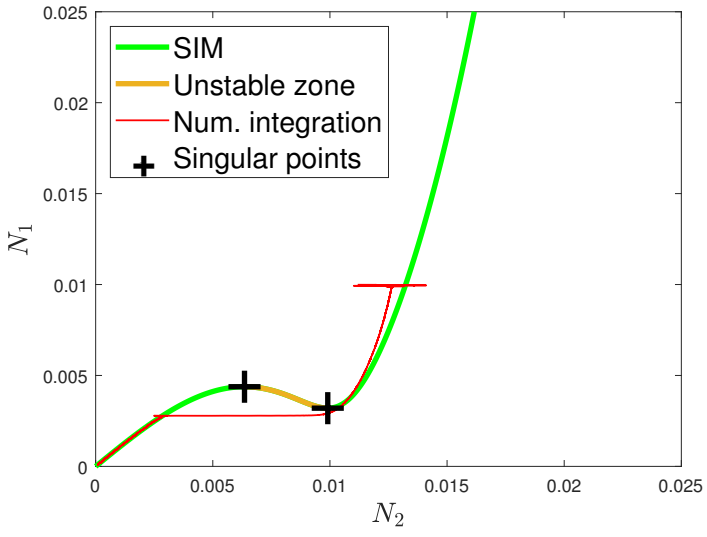

(c)

Figure 3: Free response of the cell 1 around the first mode ($k = 1$). (a) Given initial displacements reading as $u_j(\tau = 0) = 0.16\cos(\omega_1(j-1))$ for the chain; red cross symbol stands for the position of the cell 1. (b) Time histories of N_1 of the cell 1 obtained by direct numerical integration. (c) The SIM of the system (green line) accompanied by numerical results (red line). Black $+$ symbols present amplitudes of possible singularities of the system. Unstable zone of the SIM is represented in orange line. Parameters of the system are listed in configuration number 2 of Table 1.

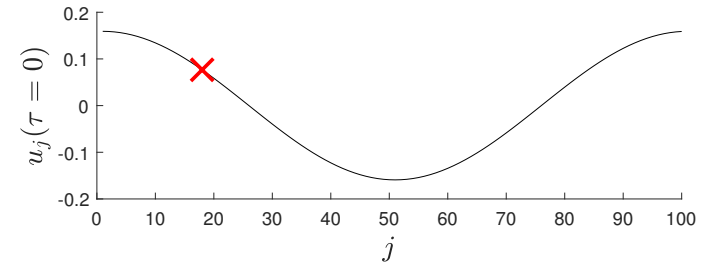

(a)

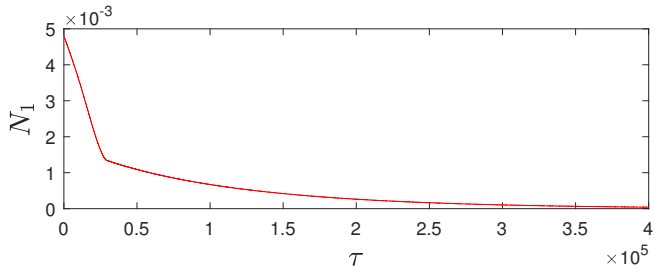

(b)

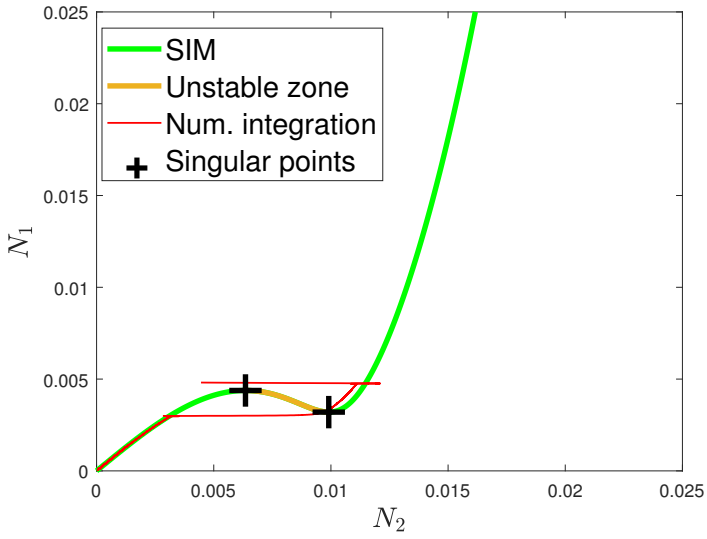

(c)

Figure 4: Free response of the cell 18 around the first mode ($k = 1$). (a) Given initial displacements reading as $u_j(\tau = 0) = 0.16\cos(\omega_1(j-1))$ for the chain; red cross symbol stands for the position of the cell 18. (b) Time histories of N_1 of the cell 18 obtained by direct numerical integration. (c) The SIM of the system (green line) accompanied by numerical results (red line). Black $+$ symbols present amplitudes of possible singularities of the system. Unstable zone of the SIM is represented in orange line. Parameters of the system are listed in configuration number 2 of Table 1.

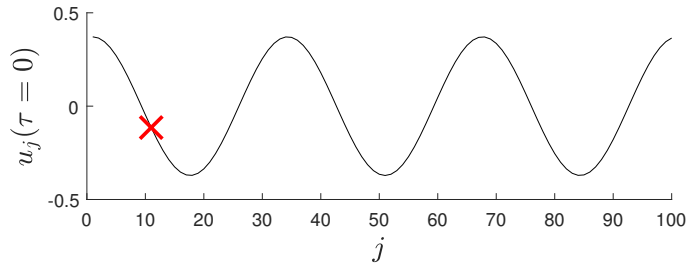

(a)

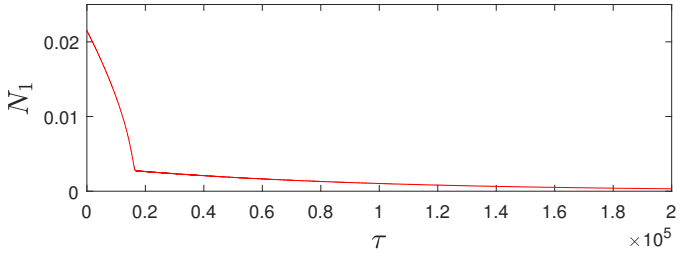

(b)

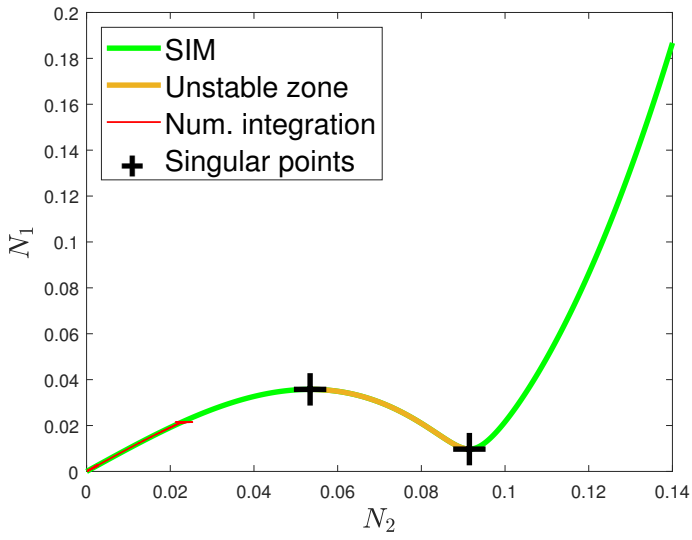

(c)

Figure 5: Free response of the cell 11 around the third mode ($k = 3$). (a) Given initial displacements reading as $u_j(\tau = 0) = 0.37\cos(\omega_3(j-1))$ for the chain; red cross symbol stands for the position of the cell 11. (b) Time histories of N_1 of the cell 11 obtained by direct numerical integration. (c) The SIM of the system (green line) accompanied by numerical results (red line). Black $+$ symbols present amplitudes of possible singularities of the system. Unstable zone of the SIM is represented in orange line. Parameters of the system are listed in configuration number 2 of Table 1.

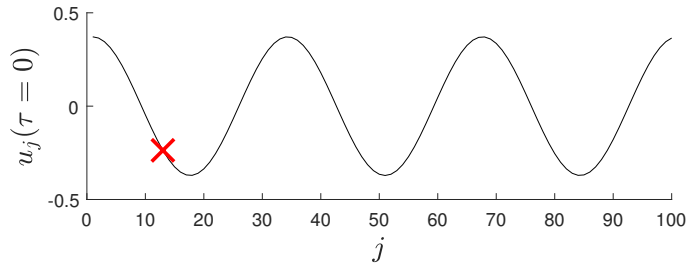

(a)

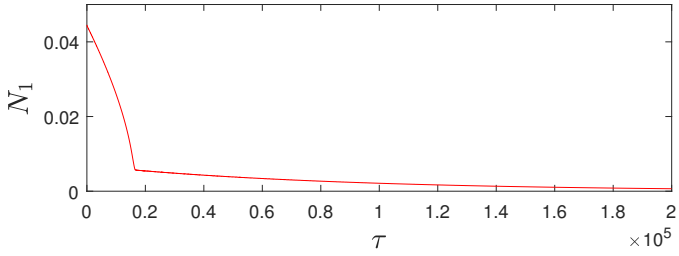

(b)

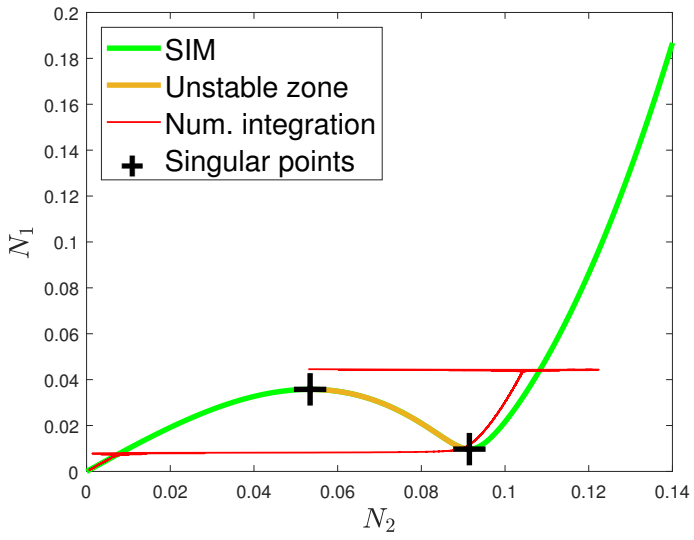

(c)

Figure 6: Free response of the cell 13 around the third mode ($k = 3$). (a) Given initial displacements reading as $u_j(\tau = 0) = 0.37\cos(\omega_3(j-1))$ for the chain; red cross symbol stands for the position of the cell 13. (b) Time histories of N_1 of the cell 13 obtained by direct numerical integration. (c) The SIM of the system (green line) accompanied by numerical results (red line). Black $+$ symbols present amplitudes of possible singularities of the system. Unstable zone of the SIM is represented in orange line. Parameters of the system are listed in configuration number 2 of Table 1.

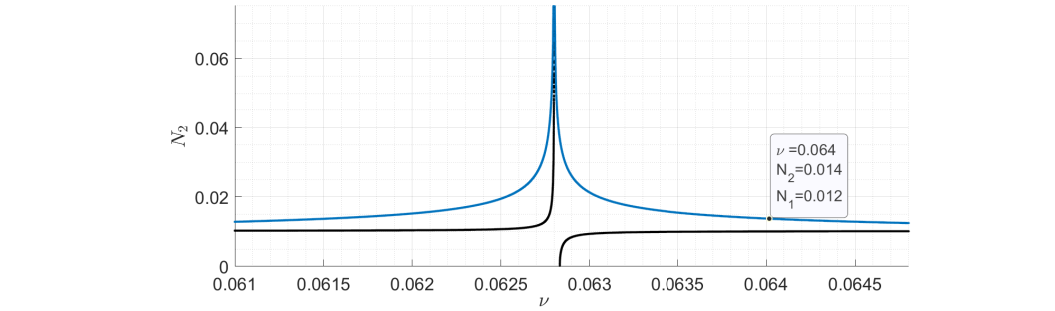

(a)

(b)

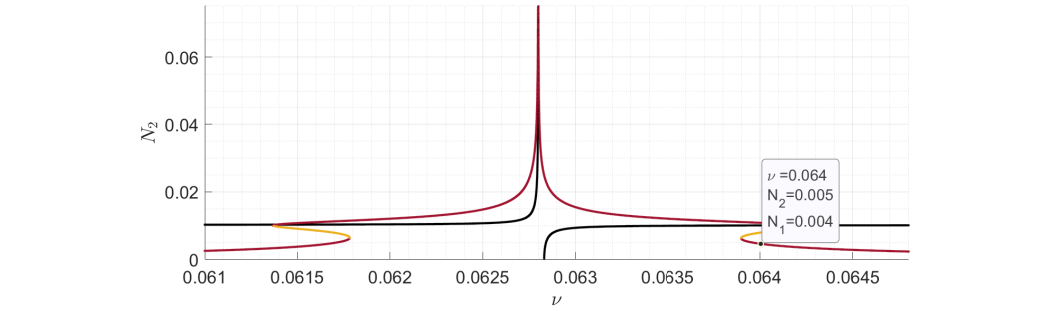

(c)

(d)

Figure 7: Forced responses of cells 1 and 21 of the chain under external forcing around the first mode ($k = 1$) with the amplitude $f_j = 0.03\cos(\omega_1(j-1))$. (a) and (c) Frequency response curves of cell 1 and cell 21 respectively. Backbone curves are represented by thick black lines while equilibrium points falling in unstable zone of the SIM are represented in orange line. (b) and (d) Time histories of amplitudes of concerned cells obtained from numerical results for system with $\nu = 0.064$ with zero initial condition. System characteristics are provided in configuration 2 of Table 1.

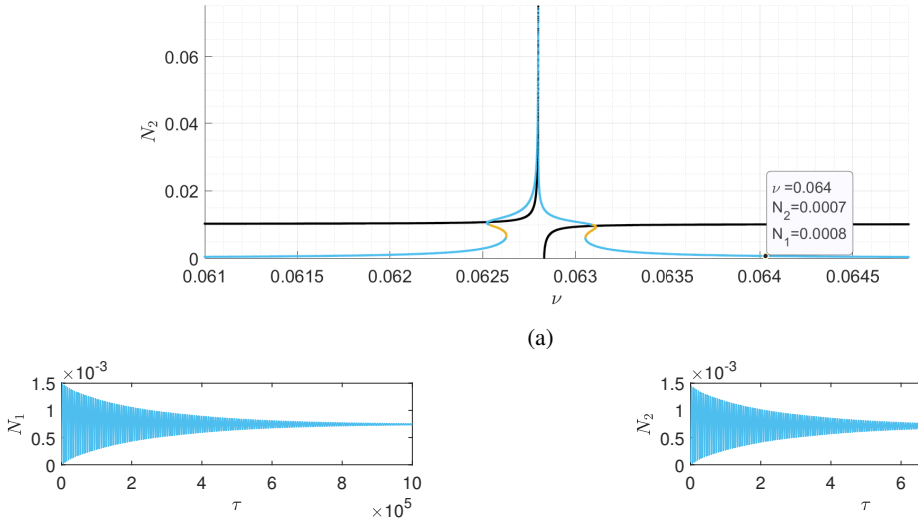

Figure 8: Forced responses of the cell 27 of the chain under external forcing around the first mode ($k = 1$) with the amplitude $f_j = 0.03\cos(\omega_1(j-1))$. (a) Frequency response curves of the cell. Backbone curves are represented by thick black lines while equilibrium points falling in unstable zone of the SIM are represented in orange line. (b) Time histories of amplitudes of the cell obtained from numerical results for system with $\nu = 0.064$ with zero initial condition. System characteristics are given in configuration 2 of Table 1.

Let us suppose the system under external excitation with the frequency around the third mode of the chain ($k = 3$). The system characteristics are presented in configuration 3 in Table 1 with forcing term $f_j = 0.01\cos(\omega_3(j-1))$ and $\nu = 0.1895$. As some representative examples, frequency response curves for different cells are presented in Fig.16a,16c and 17a, while numerical results for the system with $\nu = 0.1895$, are depicted in Fig.16b,16d and 17b. It is seen that some cells possess only one equilibrium point falling in the unstable zone of the SIM, e.g. cell 1, indicating a quasi-periodic response of the system corresponding to repeated bifurcations between stable zones of the SIM (see Fig.16b and 18a). The Poincaré map of cell 1 is depicted in Fig.20a showing quasi-periodic response of the cell. Looking at the instantaneous frequency of this cell, see Fig.21a, it is seen that this cell presents abrupt changes of frequencies due to bifurcations. Some cells possess only one equilibrium point positioned in stable zones of the SIM, for example cell 8 (see Fig.18b). The Poincaré map and instantaneous frequency of this cell depicted in Fig.20b and 21b, show the quasi-periodic response of this cell, without presence of bifurcations (see Fig.18b). Finally, some other cells can have one to three equilibrium points falling in stable and unstable zone of the SIM, for example cell 7 (see Fig.17,19,20c and 21c). The predicted behavior of the chain at its equilibrium points is represented in Fig.22 (3D view) and 23 (2D views), where blue and red diamonds are referred to maximal and minimal values of amplitude of N_1 and N_2 respectively , see also Figs.18 and 19. Numerical results are quantitatively in good agreements with predicted equilibrium points. When the system possess only one equilibrium point positioned in unstable zone of the SIM, e.g. cell 1, due to repeated bifurcations, there will be large variations of system amplitudes around predicted unstable equilibrium point. Other discrepancy between analytical and numerical results can arise from the fact that we do not consider inter-modal energy exchanges for this study.
To summarize, we can observe three different situations for each cell depending on the frequency and amplitude of the excitation:

- only one point exists out of unstable zone of the SIM;
- only one point exists inside the unstable zone of the SIM; the concerned cell will present modulated responses (25) corresponding to repeated bifurcations between stable zones of the SIM;
- two or three possible equilibrium points exist and some of them can be located in the unstable zone of the SIM.

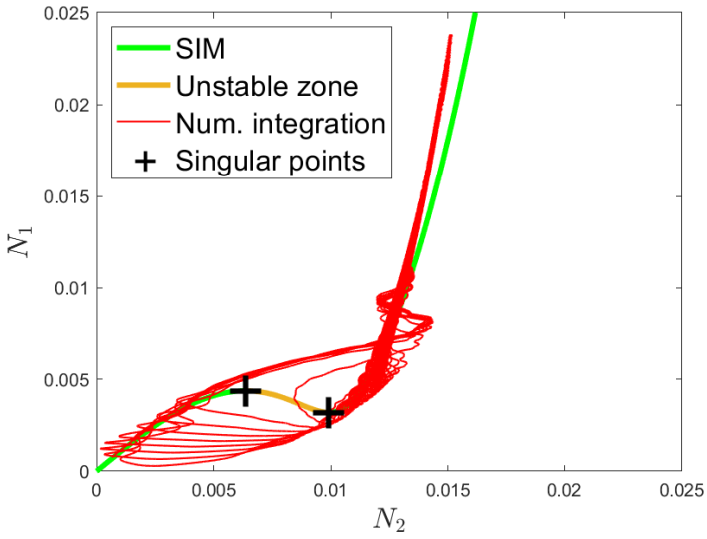

Figure 9: Forced response of the cell 1 around the first mode ($k = 1$). The SIM of the system (green line) accompanied by numerical results (red line). Black '+' symbols present amplitudes of possible singularities of the system. Unstable zone of the SIM is represented in orange line. System is under external excitation with the amplitude of $f_j = 0.03\cos(\omega_1(j-1))$ and the frequency of $\nu = 0.064$ with zero initial conditions. Parameters of the system are listed in configuration number 2 of Table 1.

5 Conclusion

Multi scale dynamics of a $2L$ degrees of freedom periodic chain has been studied. After transferring discrete coordinates to continuous domain, the nature of the solutions according to the spatial arrangement of the system is obtained. Slow invariant manifold of the system is detected at fast time scale and the behavior of the system at slow time scale is analytically expressed using multiple scale method. We are able to predict equilibrium points and singularities of the system according to excitation and the position of each cell in the chain. Plotting stability borders as a function of some design parameters permits to adapt the system for an application for example. Numerical simulations on this chosen system have confirmed our analytical predictions when the considered mode is not too high. According to the forcing term, its spatial phases and the position of the cell in the chain, the system can present one, two or three equilibrium points which can be in the stable zone of the slow invariant manifold, presenting possible periodic regimes, or in the unstable zone showing non-periodic behaviors with repeated bifurcations. Different types of behaviors can be observed along the chain at the same time depending on the position of the cells. Continuous approach of the periodic nonlinear chain of oscillators has delivered good results and should be extended to multi-modal study. The perspective of this work will be to consider modal interactions between two or several modes of the chain.

Appendix A

Continuous approach of the system with modal projection:

Let us consider the eigenfunction of the system which is defined in Eq.23. We normalize this function via

$$\int_0^L \left(\tilde{\rho}_k \cos(\omega_k x + \Theta_k)\right)^2 dx = 1 \tag{51}$$

leading to $\tilde{\rho}_k = \sqrt{2/L}$. We define:

$$\begin{cases} U(x,\tau) = \tilde{\rho}_{1,k}(\tau)\sqrt{\frac{2}{L}}\cos(\omega_k x + \Theta_k) \\ \\ V(x,\tau) = \tilde{\rho}_{2,k}(\tau)\sqrt{\frac{2}{L}}\cos(\omega_k x + \Theta_k) \end{cases} \tag{52}$$

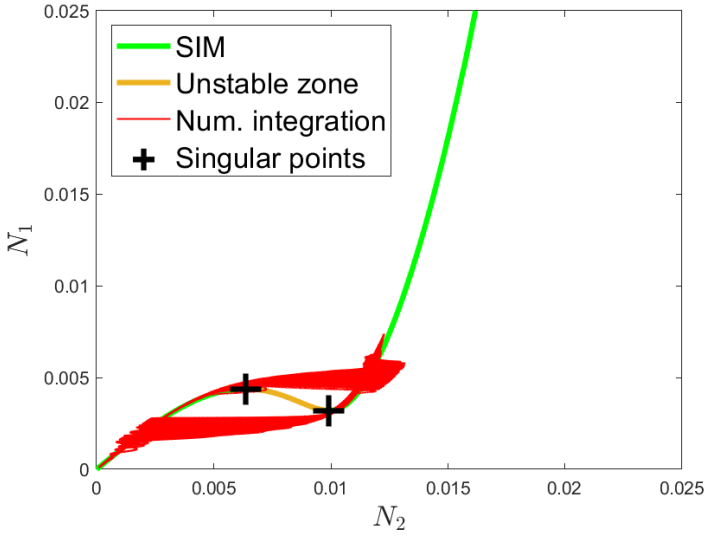

Figure 10: Forced response of the cell 21 around the first mode ($k = 1$). The SIM of the system (green line) accompanied by numerical results (red line). Black '+' symbols present amplitudes of possible singularities of the system. Unstable zone of the SIM is represented in orange line. System is under external excitation with the amplitude of $f_j = 0.03\cos(\omega_1(j-1))$ and the frequency of $\nu = 0.064$ with zero initial conditions. Parameters of the system are listed in configuration number 2 of Table 1.

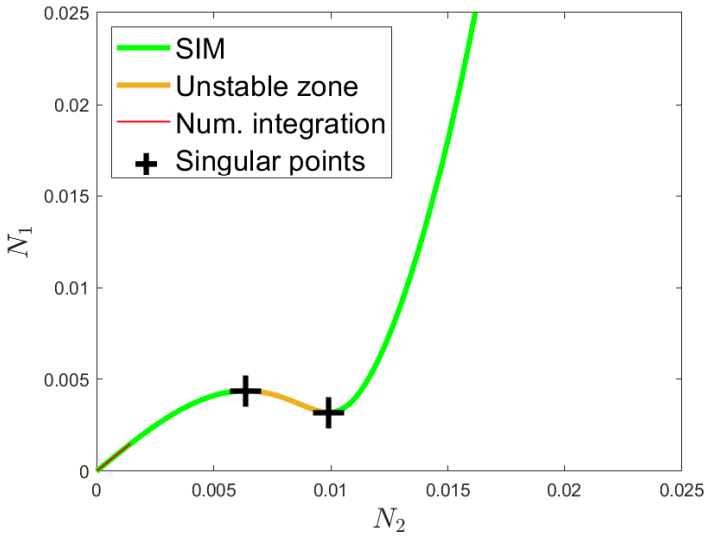

Figure 11: Forced response of the cell 27 around the first mode ($k = 1$). The SIM of the system (green line) accompanied by numerical results (red line). Black '+' symbols present amplitudes of possible singularities of the system. Unstable zone of the SIM is represented in orange line. System is under external excitation with the amplitude of $f_j = 0.03\cos(\omega_1(j-1))$ and the frequency of $\nu = 0.064$ with zero initial conditions. Parameters of the system are listed in configuration number 2 of Table 1.

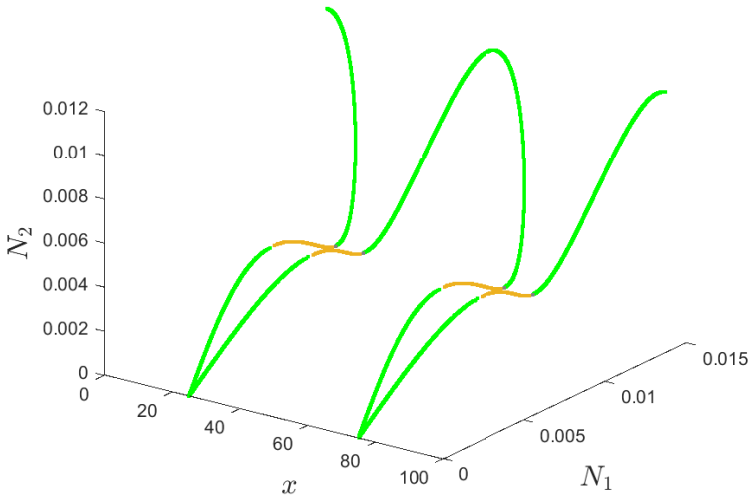

Figure 12: Analytical predictions of equilibrium points of the continuous system (green line) for system under external excitation with the amplitude of $f_j = 0.03\cos(\omega_1(j-1))$ and the frequency of $\nu = 0.064$. Unstable zone of the SIM is represented in orange line. Parameters of the system are listed in configuration number 2 of Table 1.

ω_k being defined in Eq.20.
We can project second equation of Eq.7 on the k^{th} mode as:

$$\begin{aligned}&\int_0^L \left(\tfrac{\partial^2(U-V)}{\partial\tau^2}(x,\tau) - \Lambda V^3(x,\tau) - \chi_2\tfrac{\partial V}{\partial\tau}(x,\tau)\right)\sqrt{\tfrac{2}{L}}\cos(\omega_k x + \Theta_k)dx \\ &= \tfrac{d^2\tilde{\rho}_{1,k}}{d\tau^2}(\tau) - \tfrac{d^2\tilde{\rho}_{2,k}}{d\tau^2}(\tau) - \chi_2\tfrac{d\tilde{\rho}_{2,k}}{d\tau}(\tau) - \tfrac{3\Lambda}{2L}\tilde{\rho}^3_{2,k}(\tau) = 0\end{aligned} \tag{53}$$

New complex variables of Manevitch (21) are introduced as:

$$\begin{cases} \varphi_1(\tau)e^{i\nu\tau} = \dfrac{d\tilde{\rho}_{1,k}}{d\tau}(\tau) + i\nu\tilde{\rho}_{1,k}(\tau) \\ \Psi_1(\tau)e^{i\nu\tau} = \dfrac{d\tilde{\rho}_{2,k}}{d\tau}(\tau) + i\nu\tilde{\rho}_{2,k}(\tau) \end{cases} \tag{54}$$

We are looking for the SIM and set $\nu = \omega_k$.
Taking the first harmonic of Eq.53 expressed with complex variables provides:

$$\tfrac{d}{d\tau}(\varphi_1 - \Psi_1) + i\omega_k(\varphi_1 - \Psi_1) - \chi_2\Psi_1 + \tfrac{9i\Lambda}{8L\omega_k^3}\Psi_1^2\Psi_1^* = 0 \tag{55}$$

We seek for fixed points (see Eq.30) so we can write:

$$\varphi_1 = \Psi_1 - \tfrac{i\chi_2}{2}\Psi_1 + \tfrac{9\Lambda}{8L\omega_k^4}\Psi_1^2\Psi_1^* \tag{56}$$

We introduce complex variables in polar domain as:

$$\begin{cases} \varphi_1(\tau) = \mathcal{N}_1(\tau)e^{i\vartheta_1(\tau)} \\ \Psi_1(\tau) = \mathcal{N}_2(\tau)e^{i\vartheta_2(\tau)} \end{cases} \tag{57}$$

with $\mathcal{N}_1, \mathcal{N}_2 \in \mathbb{N}^2$ and $\vartheta_1, \vartheta_2 \in \mathbb{Z}^2$. Finally, this approach leads to the SIM expression:

$$\mathcal{N}_1(\tau_1, \dots) = \sqrt{\left(\mathcal{N}_2(\tau_1, \dots) - \tfrac{9\Lambda}{8L\omega_k^4}\mathcal{N}_2^3(\tau_1, \dots)\right)^2 + \left(\tfrac{\chi_2}{\omega_k}\mathcal{N}_2(\tau_1, \dots)\right)^2} \tag{58}$$

The SIM does not depend to space variable x because of the modal projection. The expression is compared to numerical results using Runge Kutta algorithm in free and forced cases using the same methodology as in Sec.4.
In the free case shown in Fig.24 for the first mode ($k = 1$) and for the same physical parameters listed in configuration

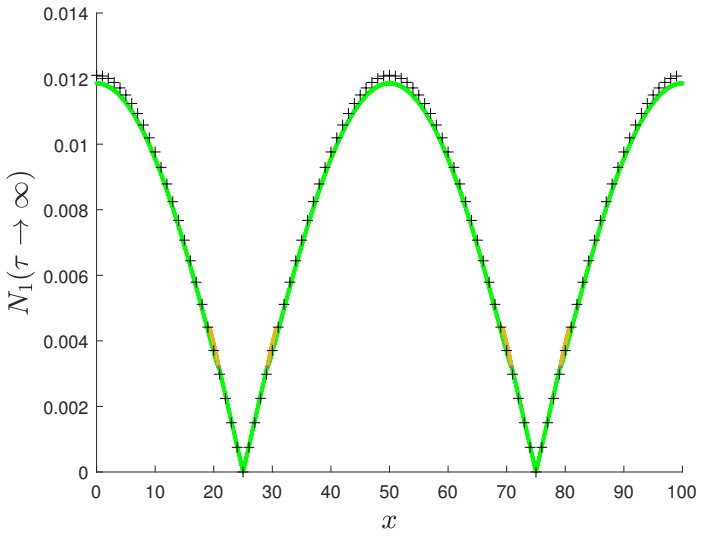

(a)

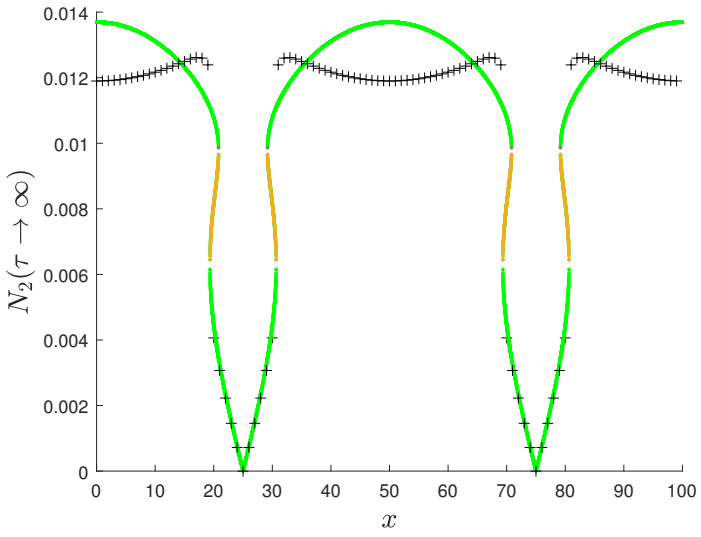

(b)

Figure 13: Analytical predictions of equilibrium points of the continuous system (green line) accompanied by those obtained from direct numerical integration (black '+' symbols) when $\tau \to \infty$ ($\tau > 9.988 \times 10^5$) with zero initial conditions under external excitation with the amplitude of $f_j = 0.03\cos(\omega_1(j-1))$ and the frequency of $\nu = 0.064$. Unstable zone of the SIM is represented in orange line. Parameters of the system are listed in configuration number 2 of Table 1.

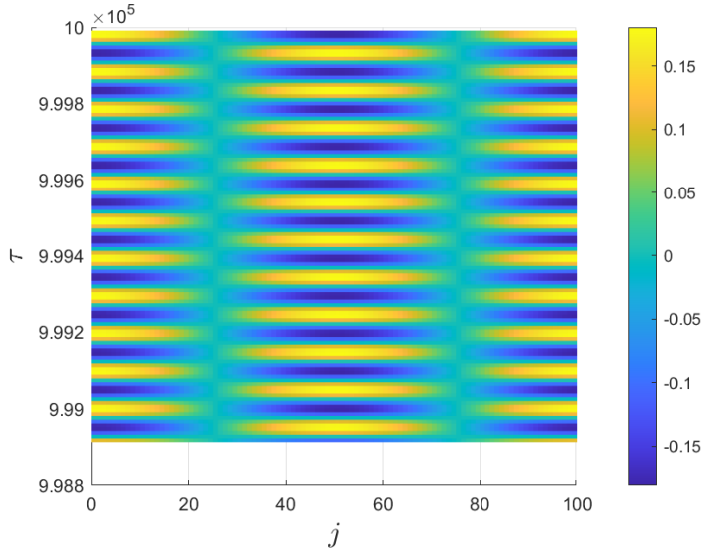

Figure 14: Periodic variations of $u_j(\tau)$ of the discrete system (numerical results) for different j ($j = x + 1$) around equilibrium points of the system with zero initial condition under external excitation with the amplitude of $f_j = 0.03\cos(\omega_1(j-1))$ and the frequency of $\nu = 0.064$ when $\tau \to \infty$ ($\tau > 9.988 \times 10^5$). Parameters of the system are listed in configuration number 2 of Table 1.

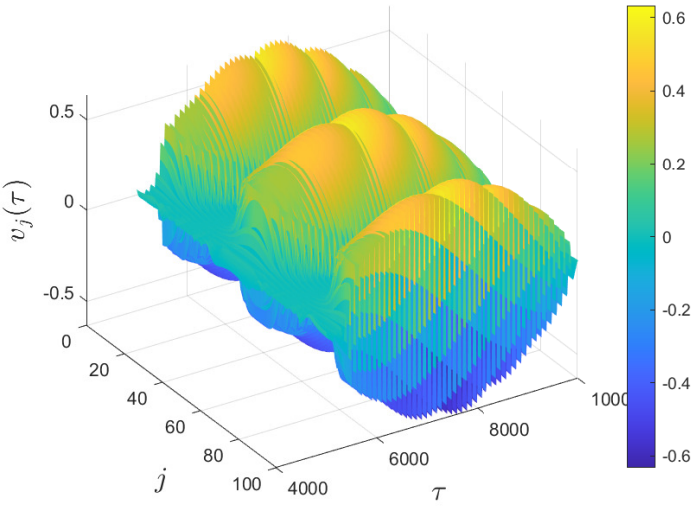

Figure 15: Transient response of $v_j(\tau)$ ($j = x + 1$) of the discrete system (numerical results). Some cells present modulated responses before going to the equilibrium point which is represented in Fig.13(b). System is under external excitation with the amplitude of $f_j = 0.03\cos(\omega_1(j-1))$ and frequency of $\nu = 0.064$ with zero initial conditions. Parameters of the system are listed in configuration number 2 of Table 1.

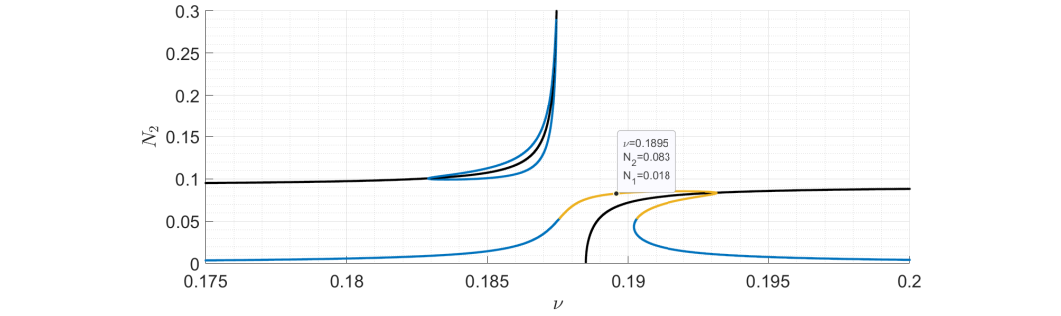

(a)

(b)

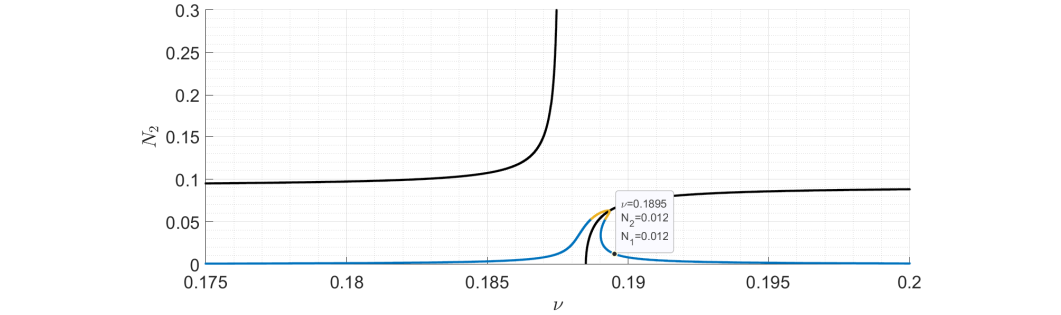

(c)

(d)

Figure 16: Forced responses of the cells 1 and 8 of the chain under external forcing around the third mode ($k = 3$) with the amplitude of $f_j = 0.01\cos(\omega_3(j-1))$. (a) and (c) Frequency response curves of the cells 1 and 8 respectively. Backbone curves are represented by thick black lines while equilibrium points falling in unstable zone of the SIM are represented in orange line. (b) and (d) Time histories of amplitudes of concerned cells obtained from numerical results for system with the frequency of $\nu = 0.1895$ and zero initial condition. System characteristics are given in configuration 3 in Table 1.

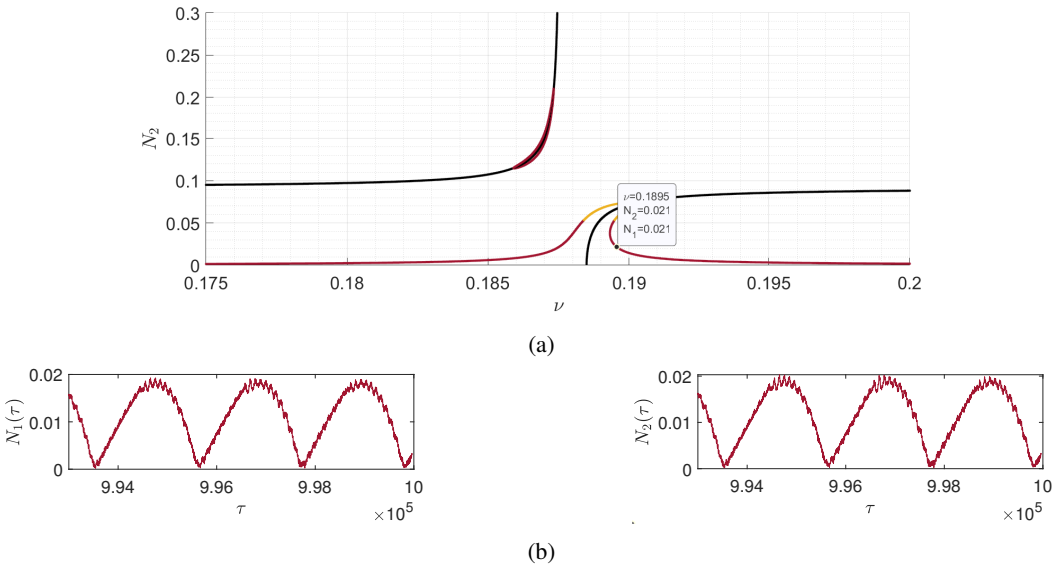

Figure 17: Forced responses of the cell 7 of the chain under external forcing around the third mode ($k = 3$) with the amplitude of $f_j = 0.01\cos(\omega_3(j-1))$. (a) Frequency response curve of the cell. Backbone curves are represented by thick black lines while equilibrium points falling in unstable zone of the SIM are represented in orange line. (b) Time histories of amplitudes obtained from numerical results for system with the frequency of $\nu = 0.1895$ and zero initial condition. System characteristics are given in configuration 3 in Table 1.

2 in Table 1 and initial deformation defined as $u_j(\tau = 0) = 0.13\cos(\omega_1(j-1))$, we can observe that the numerical results (in red line) are not really following the SIM (in green line) defined in Eq.58 except in the part close to $\mathcal{N}_1(\tau) = \mathcal{N}_2(\tau) = 0$, when all masses are in small displacements and system behave in a classical manner. We can observe that there are jumps in the numerical curve creating steps like aspect on the curve. In fact, these jumps correspond to the crossing of some cells through one bifurcation point. Indeed, each cell is at a different level of energy characterized by different amplitudes of $N_1(x,\tau)$ and $N_2(x,\tau)$, as defined in first part in Eq.27. For this reason, each cell is susceptible to cross through bifurcation points at different instants than another cells. When projecting on the mode, if some of the cells are in the unstable zone, then when a cell faces a bifurcation point, there will be a jump in the numerical curve obtained after modal projection. This phenomena is the cause of the gap between the numerical integration and the SIM that is appearing "step by step" like on the numerical curve. This is confirmed by superposing time history of numerically obtained $\sqrt{\frac{2}{L}}\mathcal{N}_2(\tau)$ of projected discrete system with different numerically obtained discrete $N_2(x = j,\tau)$ time histories of twenty five first cells of the chain in Fig.25. This figure illustrates well the influence of each cell on the modal projection results.
Same results are observable in the forced case: when forcing is added to the system, the numerical results are also less in agreement with the SIM except in the part close to $\mathcal{N}_1(\tau) = \mathcal{N}_2(\tau) = 0$, when all masses are in small displacements and system behave in classical manner, as shown in Fig.26 for excitation around the third modal frequency ω_3. This time, jumps happen around the first bifurcation point (N_{21}, N_{11}) for some cells creating the visible non-regularities on the numerical curve obtained after modal projection of discrete system in Fig.26. This is confirmed in Fig.29 where time history of numerically obtained $\sqrt{\frac{2}{L}}\mathcal{N}_2(\tau)$ of projected discrete system is compared to numerically obtained discrete $N_2(x = j,\tau)$ time histories of twenty five first cells of the chain. Moreover, when some cell amplitudes of the chain are in the unstable zone of the SIM while others are behaving in a classical manner, Fig.29 permits to understand that the modal projection is less effective because it has to traduce two different types of behaviors at the same time. When all cells are behaving in a classical manner close to $N_1 = N_2 = 0$ or at high amplitudes, spatial projection will provide good results, but does not have advantages in the analytical study compared to study in Sec.3 while considering only one mode. We can remark for example from Fig.29 that the numerical curve obtain after modal projection won't be in agreement with the SIM when the distribution of the number of cells behaving in a classical manner close to $N_1 = N_2 = 0$ and the number of cell having a modulated response is equitable. The SIM obtained without projection of the continuous system provides better results (see Fig.27,28).
For these reasons, the initial study has been conducted without modal projection.

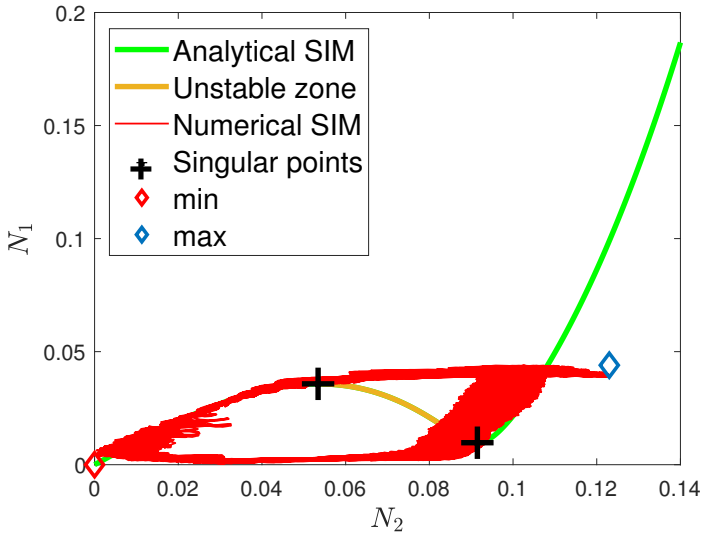

(a)

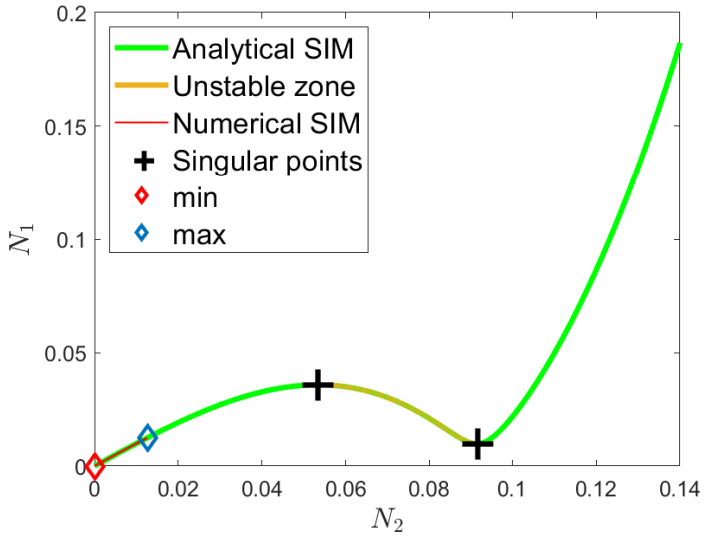

(b)

Figure 18: Forced response of the cell 1 in (a) and cell 8 in (b) around the third ($k = 3$). The SIM of the system (green line) accompanied by numerical results (red line). Black '+' symbols present amplitudes of possible singularities of the system. Unstable zone of the SIM is represented in orange line. Blue and red diamonds indicate maximal and minimal values of N_1 and N_2 respectively. System under external excitation with the amplitude of $f_j = 0.01\cos(\omega_3(j-1))$ and the frequency of $\nu = 0.1895$ with zero initial condition. Parameters of the system are listed in configuration number 3 of Table 1.

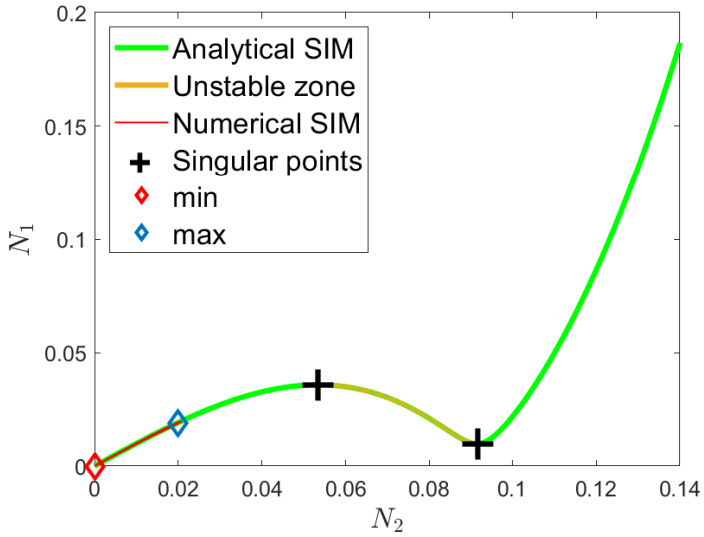

Figure 19: Forced response of the cell 7 around the third mode ($k = 3$). The SIM of the system (green line) accompanied by numerical results (red line). Black '+' symbols present amplitudes of possible singularities of the system. Unstable zone of the SIM is represented in orange line. Blue and red diamonds indicate maximal and minimal values of N_1 and N_2. System under external excitation with the amplitude of $f_j = 0.01\cos(\omega_3(j-1))$ and the frequency of $\nu = 0.1895$ with zero initial condition. Parameters of the system are listed in configuration number 3 of Table 1.

Appendix B: discrete consideration of the system

General analytical determination of discrete system modes

In this part, we are a providing the dynamical study in a discrete way. Let us consider the L-cell discrete system described in Eq.2. We express the system in the matrix form. The study is limited to the order ε^0. Eq.2 has the matrix form:

$$\begin{cases} \frac{d^2\mathbf{U}}{d\tau^2}(\tau) + \mathbf{M}_L.\mathbf{U} = 0 \\ \\ \frac{d^2\mathbf{U}}{d\tau^2}(\tau) - \frac{d^2\mathbf{V}}{d\tau^2}(\tau) - \Lambda\,\mathbf{V}^3(\tau) - \chi_2\frac{d\mathbf{V}}{d\tau}(\tau) = 0 \\ \\ \mathbf{U}_j(\tau) = u_j(\tau),\ \mathbf{V}_j(\tau) = u_j(\tau) - v_j(\tau) \text{ and } \mathbf{V}_j^3(\tau) = (u_j(\tau) - v_j(\tau))^3 \\ \\ \mathbf{M}_L = \begin{pmatrix} 2 & -1 & 0 & & & \dots & & 0 & -1 \\ -1 & 2 & -1 & 0 & & \dots & & & 0 \\ 0 & 0 & \ddots & \ddots & \ddots & 0 & & \dots & 0 \\ 0 & \dots & 0 & -1 & 2 & -1 & 0 & \dots & 0 \\ 0 & \dots & 0 & 0 & & \ddots & \ddots & \ddots & 0 \\ 0 & & & \dots & & 0 & -1 & 2 & -1 \\ -1 & 0 & & \dots & & & 0 & -1 & 2 \end{pmatrix} \text{ a } L \times L \text{ matrix} \end{cases} \tag{59}$$

Following the same procedure as described in Eq.14,15, the linearized system reads:

$$\begin{cases} \frac{d^2\mathbf{U}_l}{d\tau^2} = -\lambda.\mathbf{U}_l = -\mathbf{M}_L.\mathbf{U}_l \text{ or } \mathbf{A}_L.\mathbf{U}_l = (\mathbf{M}_L - \lambda.\mathbf{Id}_L).\mathbf{U}_l = 0 \\ \\ \mathbf{U}_l(\tau) = \begin{pmatrix} u_1 \\ \vdots \\ u_L \end{pmatrix} e^{i\sqrt{\lambda}\tau} \end{cases} \tag{60}$$

$\mathbf{Id}_L$ being the LxL identity matrix. In order to use modal projection, we are interested by the eigenvalues and eigenvectors of the matrix $\mathbf{M}_L$.

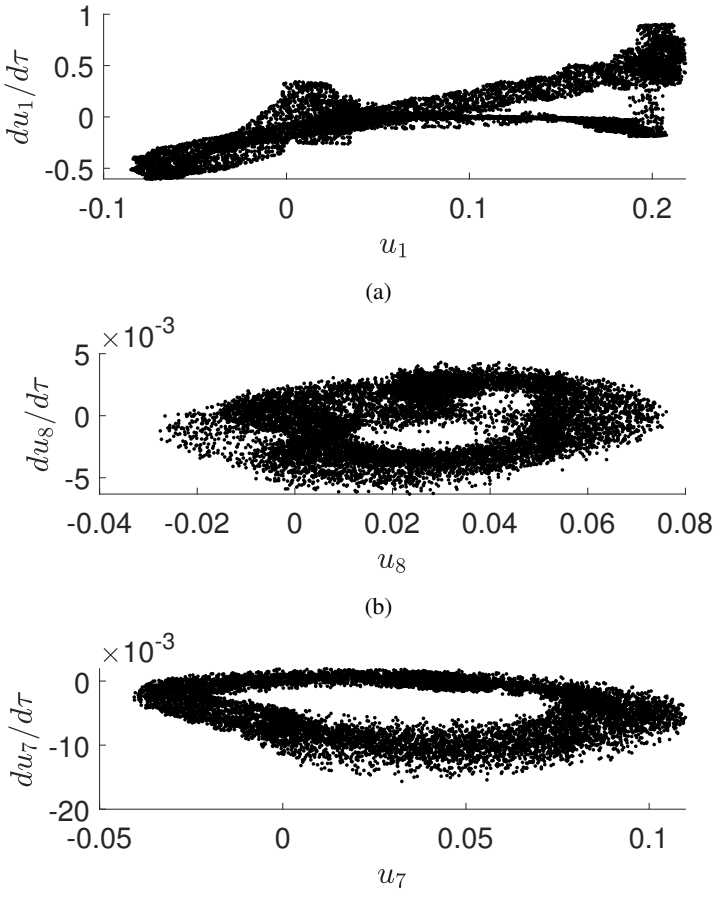

Figure 20: Poincaré diagrams (u_j versus $\frac{du_j}{d\tau}$, $j \in \{1, 8, 7\}$): (a) cell 1; (b) cell 8; (c) cell 7. System is under external excitation with the amplitude of $f_j = 0.01\cos(\omega_3(j-1))$ and the frequency of $\nu = 0.1895$ with zero initial condition. Parameters of the system are listed in configuration number 3 of Table 1.

Let us evaluate eigenvalues of $\mathbf{M}_L$. For this purpose, we define the tri-diagonal matrix:

$$\mathbf{B}_L = \begin{pmatrix} \alpha & -1 & 0 & \dots & 0 \\ -1 & \alpha & -1 & \ddots & \vdots \\ 0 & \ddots & \ddots & \ddots & 0 \\ \vdots & \ddots & -1 & \alpha & -1 \\ 0 & \dots & 0 & -1 & \alpha \end{pmatrix}_{L\times L} \tag{61}$$

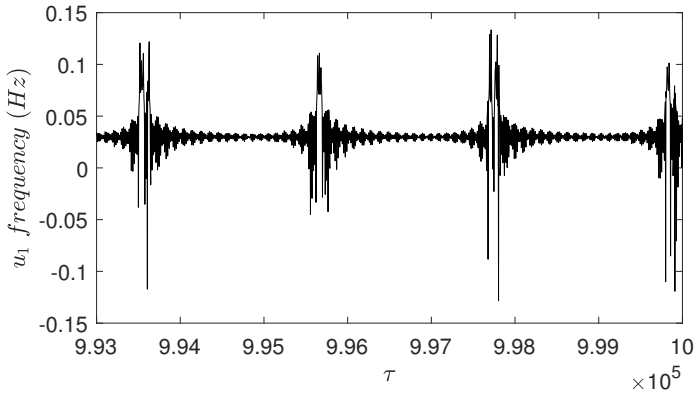

(a)

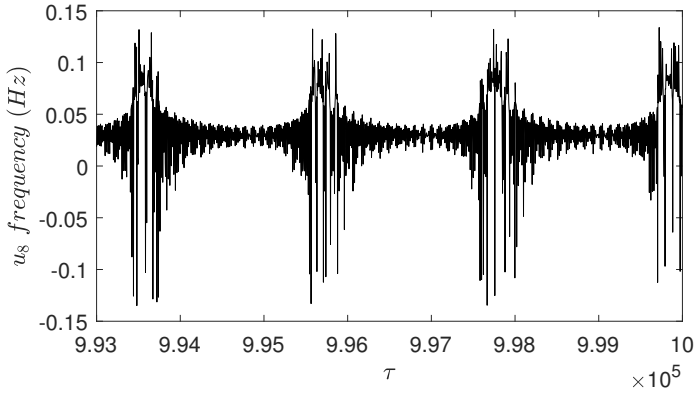

(b)

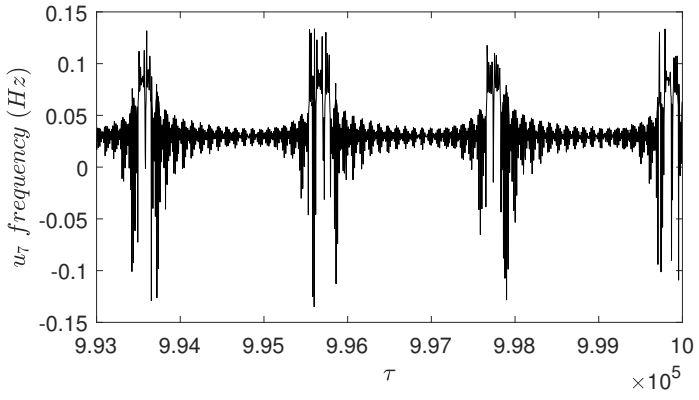

(c)

Figure 21: Instantaneous frequency of m_1 located at different positions. (a) cell 1; (b) cell 8; (c) cell 7. System is under external excitation with the amplitude of $f_j = 0.01\cos(\omega_3(j-1))$ and the frequency of $\nu = 0.1895$ with zero initial condition. Parameters of the system are listed in configuration number 3 of Table 1.

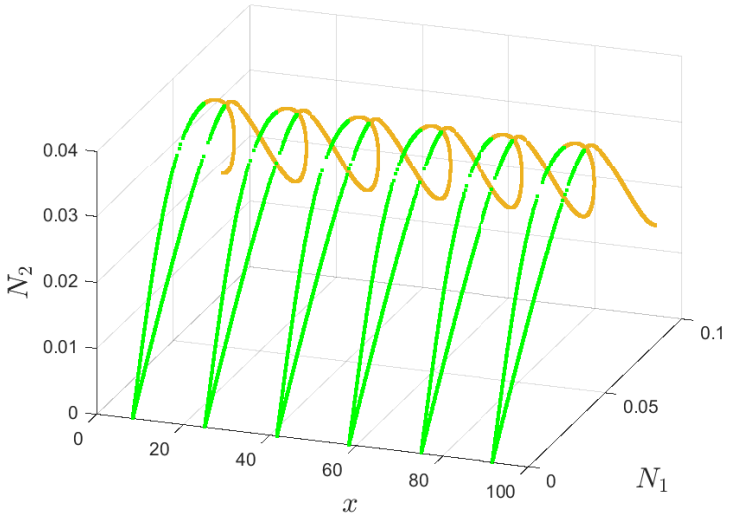

Figure 22: Analytical predictions of equilibrium points of the continuous system (green line) for system under external excitation with the amplitude of $f_j = 0.01\cos(\omega_3(j-1))$ and the frequency of $\nu = 0.1895$. Unstable zone of the SIM is represented in orange line. Parameters of the system are listed in configuration number 3 of Table 1.

We define $\alpha = 2 - \lambda$ and using Gauss pivoting methodology, we decompose:

$$\det(\mathbf{A}_L) = \alpha.\det(\mathbf{B}_{L-1}) - (-1)^3\det\left(\begin{pmatrix} -1 & -1 & 0 & \dots & \dots & 0 \\ 0 & \alpha & -1 & 0 & & \vdots \\ 0 & -1 & \alpha & -1 & \ddots & \vdots \\ \vdots & \ddots & \ddots & \ddots & \ddots & 0 \\ 0 & \dots & 0 & -1 & \alpha & -1 \\ -1 & \dots & \dots & 0 & -1 & \alpha \end{pmatrix}_{L-1\times L-1}\right) \tag{62}$$
$$-(-1)^{L+1}\det\left(\begin{pmatrix} -1 & \alpha & -1 & 0 & \dots & 0 \\ 0 & -1 & \alpha & -1 & \ddots & \vdots \\ \vdots & \ddots & \ddots & \ddots & \ddots & 0 \\ \vdots & & \ddots & \ddots & \ddots & -1 \\ 0 & \dots & \dots & 0 & -1 & \alpha \\ -1 & \dots & \dots & \dots & 0 & -1 \end{pmatrix}_{L-1\times L-1}\right)$$

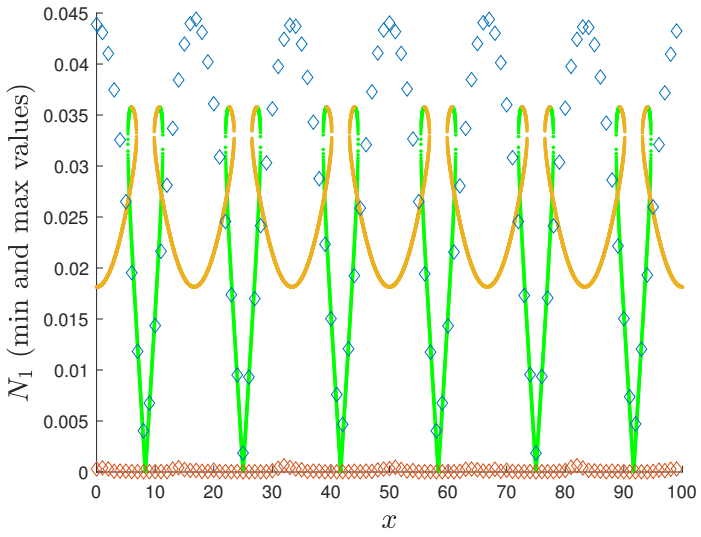

(a)

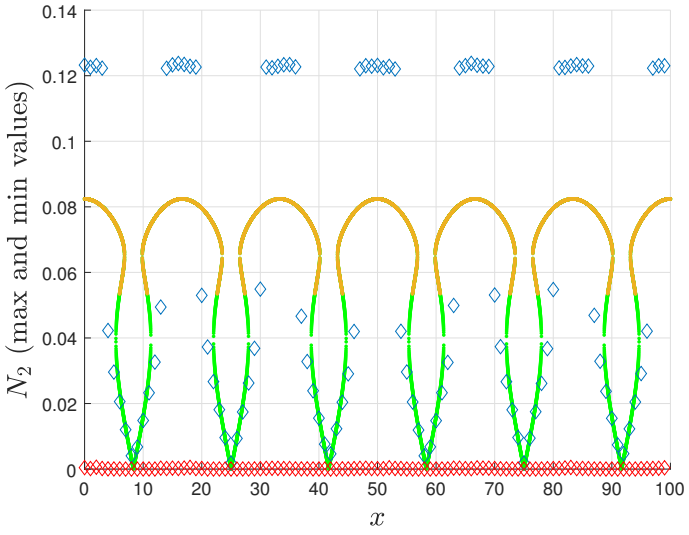

(b)

Figure 23: Analytical predictions of equilibrium points of the continuous system (green line) accompanied by those obtained from direct numerical integration (blue and red diamonds indicate maximal and minimal values of N_1 and N_2). Unstable zone of the SIM is represented in orange line. System is under external excitation with the amplitude of $f_j = 0.01\cos(\omega_3(j-1))$ and the frequency of $\nu = 0.1895$ with zero initial condition. Parameters of the system are listed in configuration number 3 of Table 1.

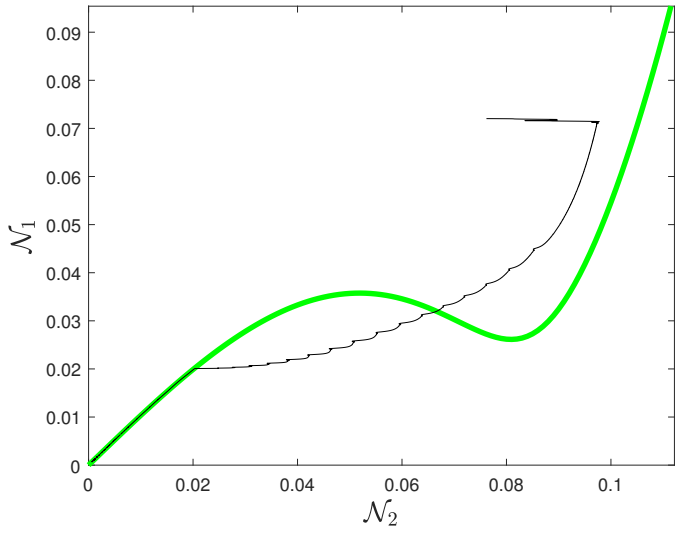

Figure 24: The SIM of the continuous system after projection on its first mode ($k = 1$), see Eq.58, accompanied by numerical results. Numerical data are collected by projections of results (obtained from direct numerical integration of Eq.2) on the first mode. Initial conditions are $u_j(\tau = 0) = 0.13\cos(\omega_1(j-1))$ with $f_j = 0$. System characteristics are listed in configuration 2 of Table 1.

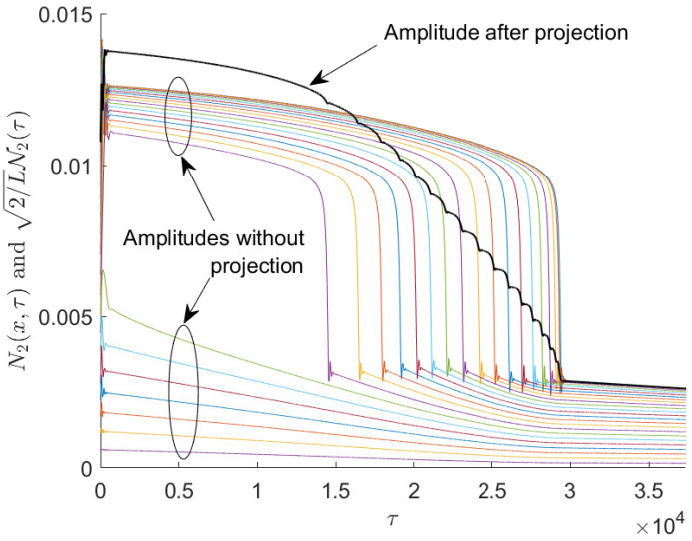

Figure 25: Time histories of $\sqrt{2/L}\mathcal{N}_2(\tau)$ of the projected discrete system accompanied by those of $N_2(x = j, \tau)$, $j = 1, \ldots, 25$ of discrete system. $\mathcal{N}_2(\tau)$ numerical data are collected by projections of results (obtained from of direct numerical integration of Eq.2) on the first mode. Definition of $N_2(\tau)$ and $\mathcal{N}_2(\tau)$ are in Eq.27 and Eq.57 respectively. Initial conditions are $u_j(\tau = 0) = 0.13\cos(\omega_1(j-1))$ with $f_j = 0$. System characteristics are listed in configuration 2 of Table 1.

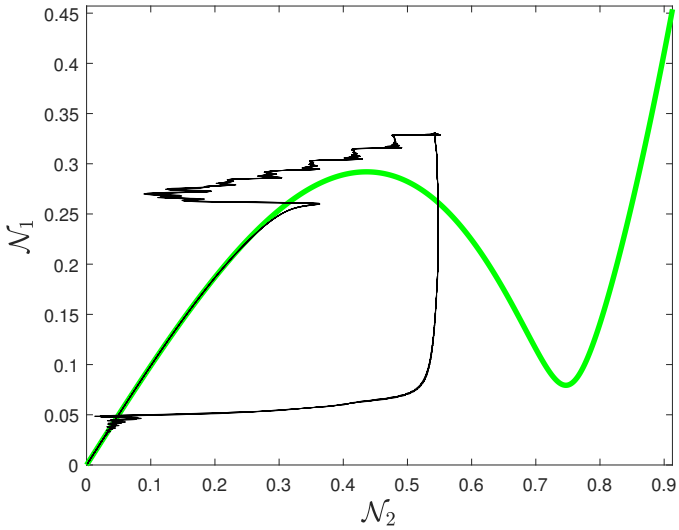

Figure 26: SIM of the continuous system after projection on third mode ($k = 3$) in green line accompanied by numerical results of discrete system during repeated bifurcations. Numerical data are collected by projections of results (obtained from of direct numerical integration of Eq.2) on third mode. External excitation has an amplitude $f_j = 0.02\cos(\omega_3(j-1))$ with frequency $\nu = 0.1885$ and zero initial conditions. System characteristics are listed in configuration 2 in Table 1.

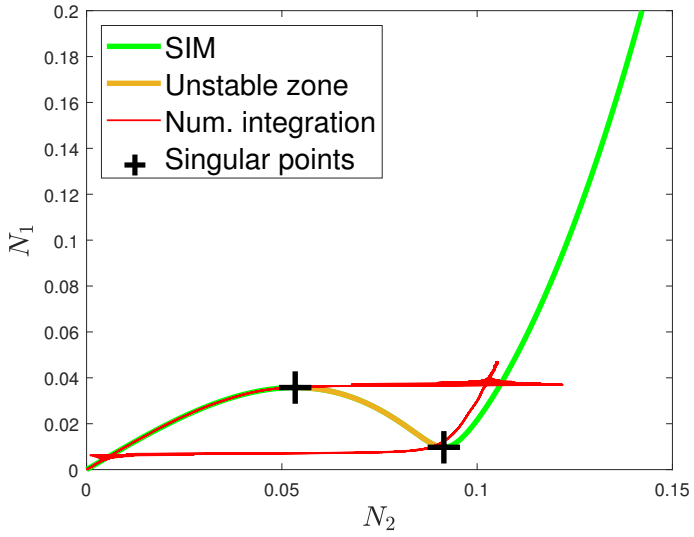

Figure 27: Forced response of the cell 1 around the first mode ($k = 1$). The SIM of the system (green line) accompanied by numerical results (red line) during repeated bifurcations. Black + symbols present amplitudes of possible singularities of the system. Unstable zone of the SIM is represented in orange line. System is under external excitation with the amplitude of $f_j = 0.02\cos(\omega_3(j-1))$ and the frequency of $\nu = 0.1885$ with zero initial condition. System characteristics are listed in configuration 2 of Table 1.

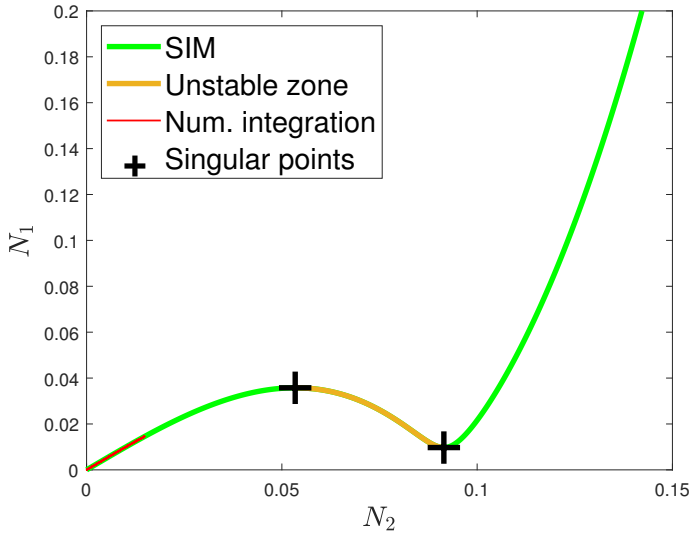

Figure 28: Forced response of the cell 11 around the first mode ($k = 1$). The SIM of the system (green line) accompanied by numerical results (red line). Black $+$ symbols present amplitudes of possible singularities of the system. Unstable zone of the SIM is represented in orange line. System is under external excitation with the amplitude of $f_j = 0.02\cos(\omega_3(j-1))$ and the frequency of $\nu = 0.1885$ with zero initial condition. System characteristics are listed in configuration 2 of Table 1.

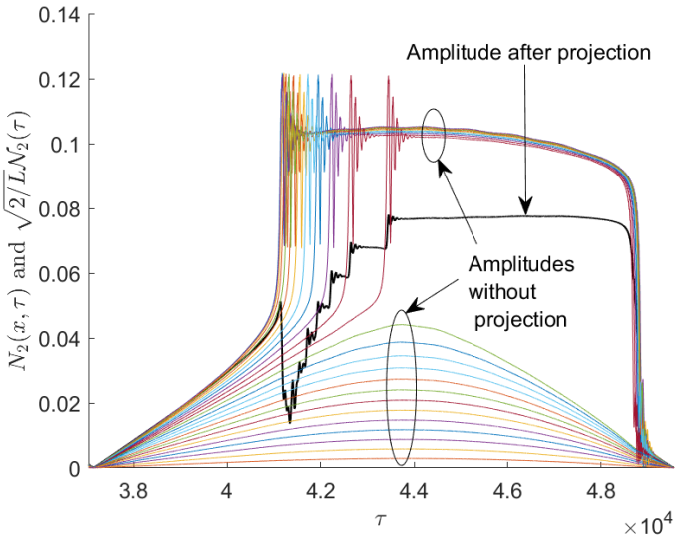

Figure 29: Time histories of $\sqrt{2/L}\mathcal{N}_2(\tau)$ of the projected discrete system accompanied by those of $N_2(x = j, \tau)$, $j = 1, \ldots, 25$ of discrete system. $\mathcal{N}_2(\tau)$ numerical data are collected by projections of results (obtained from of direct numerical integration of Eq.2) on the third mode. System is under external excitation with the amplitude of $f_j = 0.02\cos(\omega_3(j-1))$ and the frequency of $\nu = 0.1885$ with zero initial condition. System characteristics are listed in configuration 2 of Table 1.

where:

$$\det\begin{pmatrix} -1 & -1 & 0 & \dots & \dots & 0 \\ 0 & \alpha & -1 & 0 & & \vdots \\ 0 & -1 & \alpha & -1 & \ddots & \vdots \\ \vdots & \ddots & \ddots & \ddots & \ddots & 0 \\ 0 & \dots & 0 & -1 & \alpha & -1 \\ -1 & \dots & \dots & 0 & -1 & \alpha \end{pmatrix}_{L-1\times L-1} = (-1)\det(\mathbf{B}_{L-2}) +$$

$$(-1)(-1)^L \det\begin{pmatrix} -1 & 0 & 0 & \dots & \dots & 0 \\ \alpha & -1 & 0 & & & \vdots \\ -1 & \alpha & -1 & \ddots & & \vdots \\ 0 & \ddots & \ddots & \ddots & \ddots & 0 \\ \vdots & \ddots & \ddots & \ddots & \ddots & 0 \\ 0 & \dots & 0 & -1 & \alpha & -1 \end{pmatrix}_{L-2\times L-2} \tag{63}$$

$$= -\det(\mathbf{B}_{L-2}) + (-1)^{2L-1} = -\det(\mathbf{B}_{L-2}) - 1$$

and:

$$\det\begin{pmatrix} -1 & \alpha & -1 & 0 & \dots & 0 \\ 0 & -1 & \alpha & -1 & \ddots & \vdots \\ \vdots & \ddots & \ddots & \ddots & \ddots & 0 \\ \vdots & & \ddots & \ddots & \ddots & -1 \\ 0 & \dots & \dots & 0 & -1 & \alpha \\ -1 & \dots & \dots & \dots & 0 & -1 \end{pmatrix}_{L-1\times L-1} = -1(-1)^L \det(\mathbf{B}_{L-2}) +$$

$$(-1)\det\begin{pmatrix} -1 & \alpha & -1 & 0 & \dots & 0 \\ 0 & -1 & \alpha & -1 & \ddots & \vdots \\ \vdots & \ddots & \ddots & \ddots & \ddots & 0 \\ \vdots & & \ddots & \ddots & \ddots & -1 \\ \vdots & & & \ddots & \ddots & \alpha \\ 0 & \dots & \dots & \dots & 0 & -1 \end{pmatrix}_{L-2\times L-2} \tag{64}$$

$$= (-1)^{L+1}\det(\mathbf{B}_{L-2}) + (-1)(-1)^{L-2} = (-1)^{L+1}\det(\mathbf{B}_{L-2}) + (-1)^{L-1}$$

Finally, by re-injecting in Eq.62 the previous simplified determinants, the following simple expression is obtained:

$$\det(\mathbf{A}_L) = \alpha.\det(\mathbf{B}_{L-1}) - 2(\det(\mathbf{B}_{L-2}) + 1) \tag{65}$$

Let us now evaluate $D_L = \det(\mathbf{B}_L)$. In order to obtain non-trivial solutions of the system, we have to verify $\det(\mathbf{A}_L) = 0$. Therefore, Eq.65 leads to a second degree characteristic polynomial and we set the general expression of the solutions of the constant recursive sequence:

$$D_L = \Gamma {X_1}^n + \Sigma {X_2}^n, \{\Gamma, \Sigma\} \in \mathbb{C}^2, n \in \mathbb{N} \tag{66}$$

where X_1 and X_2 are the solutions of the characteristic polynomial.
We have the firsts relations:

$$\begin{cases} D_0 = \Gamma + \Sigma = 1 \\ D_1 = \Gamma X_1 + \Sigma X_2 = \alpha \end{cases} \tag{67}$$

Solving the system up to higher orders shows that X_1 and X_2 can't have real expressions. Therefore, X_1 and X_2 must be conjugated complexes and we use polar expressions for the two unknowns:

$$\begin{cases} X_1 = \eta e^{i\zeta} \\ X_2 = \eta e^{-i\zeta} \end{cases} \tag{68}$$

with $\eta, \zeta \in \mathbb{R}^2$. Solving Eq.67 leads to the two expressions:

$$\begin{cases} \Gamma = \frac{\alpha - \eta e^{-i\zeta}}{2i\sin(\zeta)} \\ \Sigma = -\frac{\alpha - \eta e^{i\zeta}}{2i\sin(\zeta)} \end{cases} \tag{69}$$

We can now also remark that:

$$\begin{cases} D_0 = \Gamma + \Sigma = \rho = 1 \\ D_2 = \Gamma X_1^2 + \Sigma X_2^2 = (2\alpha\cos(\zeta) - 1) = \alpha^2 - 1 \end{cases} \tag{70}$$

The solution of the second relation leads to $\alpha = 0$ or $\alpha = 2\cos(\zeta)$. Since $\alpha = 2 - \lambda$, we have the expression of the eigenvalues:

$$\lambda = 2(1 - \cos(\zeta)) \qquad \text{or} \qquad \lambda = 2 \tag{71}$$

D_L reads:

$$D_L = \frac{1}{2i\sin(\zeta)}\eta^L\left(\alpha 2i\sin(L\zeta) - \eta 2i\sin((L-1)\zeta)\right) = \frac{\sin((L+1)\zeta)}{\sin(\zeta)} \tag{72}$$

We can finally recompose the expression of det($\mathbf{A}_L$):

$$\det(\mathbf{A}_L) = \alpha\frac{\sin((L)\zeta)}{\sin(\zeta)} - 2\left(\frac{\sin((L-1)\zeta)}{\sin(\zeta)} + 1\right) = 2(\cos(L\zeta) - 1) \tag{73}$$

$\det(\mathbf{A}_L)$=0 if $\zeta = \frac{2k\pi}{L}$, $k = 0, 1, \ldots, L-1$.
According to Eq.71, we have $L+1$ equations but we only need L solutions.
The solution $\lambda = 2$ can be eliminated as general solution for every chain because it can't verify the conditions of periodicity without being linked to the number of cells of the chain (except for the solution $\lambda = 0$). However, the eigenvalue $\lambda = 2$ can be solution when $\frac{k}{L} = \frac{1}{4} \implies \zeta = \frac{\pi}{2} \implies \lambda = 2$ which in this case verifies periodicity conditions. We can conclude that all solutions can be found solving:

$$\lambda = 2(1 - \cos(\zeta)) \tag{74}$$

with $\zeta = \frac{2k\pi}{L}$, $k = 0, 1, \ldots, L-1$.
Moreover, we can remark that:

$$\cos\left(\tfrac{2k\pi}{L}\right) = \cos\left(\tfrac{2(L-k)\pi}{L}\right) \text{ for } k = 0, 1, \ldots, L-1 \tag{75}$$

Therefore, we only have $\left\lfloor \frac{L}{2} \right\rfloor + 1$ different eigenvalues, $L \in \mathbb{N}^*$. The first eigenvalue is $\lambda = 0$, corresponding to the rigid body dynamic of the chain.
The treatment of $\mathbf{M}_L.\mathbf{X} = \lambda.\mathbf{X}$ leads to the L eigenvectors. We can identify two cases:
-L is uneven, implying that the only eigenvalue associated to only one eigenvector is λ_0. Every other eigenvalues have two associated eigenvectors.
-L is even, implying that 2 eigenvalues λ_0 and $\lambda_{\lfloor L/2 \rfloor}$ have both one associated eigenvector. Every other eigenvalues have 2 associated eigenvectors.
We note $\mathbf{P}$ the orthonormal transfer matrix and we adopt the following decomposition:

$$\mathbf{P} = (\underbrace{\mathbf{P}_0}_{\lambda_0}, \underbrace{\mathbf{P}_1, \mathbf{P}_2}_{\lambda_1}, ..., \underbrace{\mathbf{P}_{2j-1}, \mathbf{P}_{2j}}_{\lambda_j}, ..., \underbrace{\mathbf{P}_L}_{\lambda_{\lfloor L/2 \rfloor} \text{ if } L \text{ is pair}}) \tag{76}$$

In all cases, we can use for the first eigenvector:

$$\mathbf{P}_0 = \sqrt{\tfrac{1}{L}}\begin{pmatrix} 1 & \ldots & 1 \end{pmatrix}^T \tag{77}$$

On the contrary, during the last mode of the chain with an even number of cells, all cells present equal amplitudes while each cell is out of phase with its neighbors. We can use:

$$\mathbf{P}_L = \sqrt{\tfrac{1}{L}}\begin{pmatrix} -1 & 1 & \ldots (-1)^j & \ldots & -1 & 1 \end{pmatrix}^T \tag{78}$$

This modal decomposition is caused by the periodicity conditions of the chain. Indeed, the decomposition of the physical behavior according to each eigenvalue needs two different eigenvectors and this joins the continuous approach: we showed that the general expression of principal displacement was $U_l(x) = A_k\cos(\omega_k x) + B_k\sin(\omega_k x)$ (see Eq.21). The determination of A_k and B_k can't be done until an excitation is applied. Therefore, the general form of expression

of deformation has to be described using $\cos(\omega_k x)$ and $\sin(\omega_k x)$ components. The same process is happening in the discrete study. Indeed, for each double eigenvalue $\lambda_k = \omega_k^2$, the 2 eigenvectors can be assimilated to $\sqrt{2/L}\cos(\omega_k x)$ and $\sqrt{2/L}\sin(\omega_k x)$, as shown on Fig.30 and 31. On the first figure, $\mathbf{P}_1$ and $\mathbf{P}_2$ are represented in red and black '+' symbols respectively while $\sqrt{2/L}\sin(\omega_1 x)$ and $\sqrt{2/L}\cos(\omega_1 x)$ are plotted in red and black respectively. On the second figure, $\mathbf{P}_5$ and $\mathbf{P}_6$ are presented in red and black '+' symbols while $\sqrt{2/L}\sin(\omega_3 x)$ and $\sqrt{2/L}\cos(\omega_3 x)$ are plotted in red and black respectively. Eigenvectors are obtained using "eig" function of Matlab® and system characteristics are configuration 1 in Table 1. Both discrete eigenvectors and continuous eigenfunctions have been normalized. Modal frequencies obtain from continuous and discrete approach are compared for different sizes of

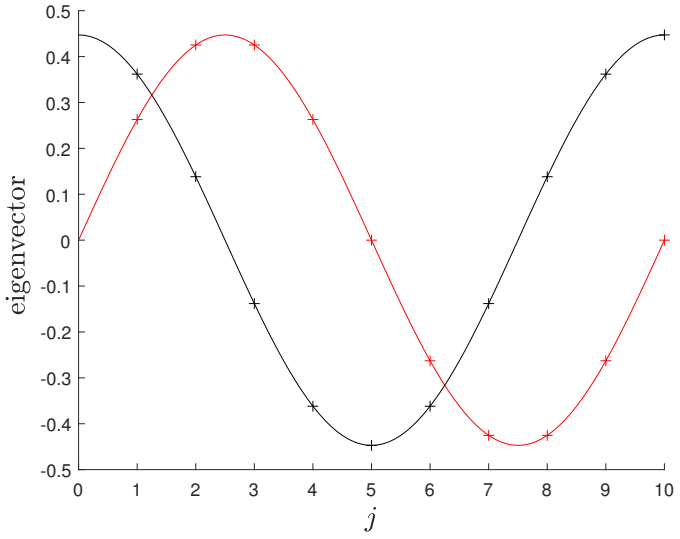

Figure 30: Comparison between eigenvectors of the discrete system at first mode ($k = 1$), $\mathbf{P}_1$ and $\mathbf{P}_2$, and components of the corresponding continuous system (see Eq.52) in the form of $\sin(\omega_1 x)$ and $\cos(\omega_1 x)$. $\mathbf{P}_1$ and $\mathbf{P}_2$ are respectively in red and black '+' symbols and normalized; $\sqrt{2/L}\sin(\omega_1 x)$ and $\sqrt{2/L}\cos(\omega_1 x)$ are represented in red and black continuous lines respectively and normalized to be compared. System characteristics are listed in configuration 1 of Table 1.

chain in Table 2. When the number of cells is high ($L = 100$ cells for example), there is a good agreement between ω_k defined in the Eq.20 and the corresponding discrete pulsation $\sqrt{\lambda_k}$. As expected, when the number of cells decreases, as well as when the considered harmonic increases, results obtained from discrete and continuous approaches depart.

Table 2: Comparison between discrete and continuous modal values

Approach	k	L=10	L=20	L=100
Discrete	1	0.618	0.313	0.0628
	2	1.176	0.618	0.126
	5	2.00	1.414	0.313
Continuous	1	0.628	0.314	0.0628
	2	1.257	0.628	0.126
	5	3.142	1.571	0.314

The SIM of the discrete chain

We can now work from second equation of Eq.59. $\mathbf{U}$ and $\mathbf{V}$ and their derivatives have the modal decomposition:

$$\begin{cases} \frac{d^n \mathbf{U}}{d\tau^n}(\tau) = \sum_j \frac{d^n \mathrm{u}_j}{d\tau^n}(\tau)\mathbf{P}_j \\ \frac{d^n \mathbf{V}}{d\tau^n}(\tau) = \sum_j \frac{d^n \mathrm{v}_j}{d\tau^n}(\tau)\mathbf{P}_j \end{cases} \tag{79}$$

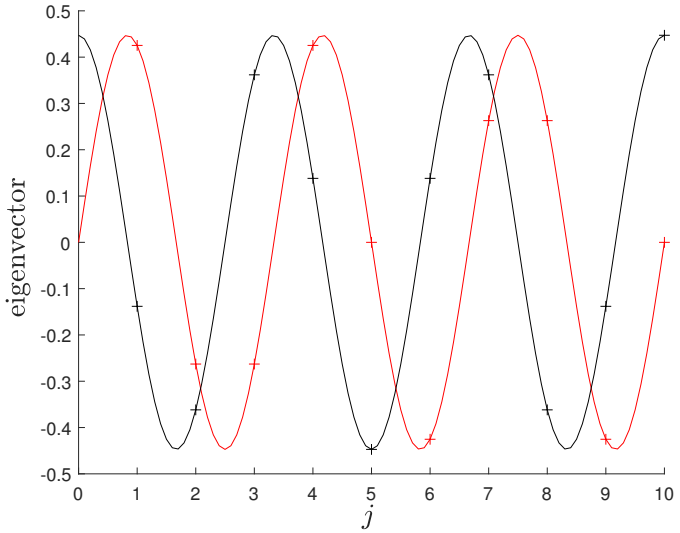

Figure 31: Comparison between eigenvectors of the discrete system at third mode ($k = 3$), $\mathbf{P}_5$ and $\mathbf{P}_6$, and components of the corresponding continuous system (see Eq.52) in the form of $\sin(\omega_3 x)$ and $\cos(\omega_3 x)$. $\mathbf{P}_5$ and $\mathbf{P}_6$ are respectively in red and black '+' symbols and normalized; $\sqrt{2/L}\sin(\omega_3 x)$ and $\sqrt{2/L}\cos(\omega_3 x)$ are represented in red and black continuous lines respectively and normalized to be compared. System characteristics are listed of configuration 1 in Table 1.

with $n \in \mathbb{N}$. In our case, we only consider one j^{th} eigenvalue:

$$\begin{cases} \frac{d^n \mathbf{U}}{d\tau^n}(\tau) = \frac{d^n \mathrm{u}_{2j-1}}{d\tau^n}(\tau)\mathbf{P}_{2j-1} + \frac{d^n \mathrm{u}_{2j}}{d\tau^n}(\tau)\mathbf{P}_{2j} \\ \frac{d^n \mathbf{V}}{d\tau^n}(\tau) = \frac{d^n \mathrm{v}_{2j-1}}{d\tau^n}(\tau)\mathbf{P}_{2j-1} + \frac{d^n \mathrm{v}_{2j}}{d\tau^n}(\tau)\mathbf{P}_{2j} \end{cases} \tag{80}$$

We project the second equation of Eq.59 on the 2 eigenvectors associated to the j^{th} eigenvalue:

$$\begin{cases} \mathbf{P}_{2j-1}^T . \left(\frac{d^2 \mathbf{U}}{d\tau^2}(\tau) - \frac{d^2 \mathbf{V}}{d\tau^2}(\tau) - \Lambda \mathbf{V}^3(\tau) - \chi_2 \frac{d\mathbf{V}}{d\tau}(\tau) \right) = 0 \\ \mathbf{P}_{2j}^T . \left(\frac{d^2 \mathbf{U}}{d\tau^2}(\tau) - \frac{d^2 \mathbf{V}}{d\tau^2}(\tau) - \Lambda \mathbf{V}^3(\tau) - \frac{d\mathbf{V}}{d\tau}(\tau) \right) = 0 \end{cases} \tag{81}$$

We can now introduce new complex variables of Manevitch (21) defined as:

$$\begin{cases} \phi_{2j-1}(\tau)e^{i\nu\tau} = \frac{d\mathrm{u}_{2j-1}}{d\tau}(\tau) + i\nu \mathrm{u}_{2j-1}(\tau) \\ \phi_{2j}(\tau)e^{i\nu\tau} = \frac{d\mathrm{u}_{2j}}{d\tau}(\tau) + i\nu \mathrm{u}_{2j}(\tau) \\ \psi_{2j-1}(\tau)e^{i\nu\tau} = \frac{d\mathrm{v}_{2j-1}}{d\tau}(\tau) + i\nu \mathrm{v}_{2j-1}(\tau) \\ \psi_{2j}(\tau)e^{i\nu\tau} = \frac{d\mathrm{v}_{2j}}{d\tau}(\tau) + i\nu \mathrm{v}_{2j}(\tau) \end{cases} \tag{82}$$

with $\nu = \sqrt{\lambda_j}$.
After keeping the first harmonic of the system, the complex variables are expressed in polar domain as:

$$\begin{cases} \phi_{2j-1}(\tau) = \mathscr{N}_{2j-1} e^{i\xi_{2j-1}} \\ \phi_{2j}(\tau) = \mathscr{N}_{2j} e^{i\xi_{2j}} \\ \psi_{2j-1}(\tau) = \mathscr{M}_{2j-1} e^{i\delta_{2j-1}} \\ \psi_{2j}(\tau) = \mathscr{M}_{2j} e^{i\delta_{2j}} \end{cases} \tag{83}$$

The methodology of the study is the same as in Sec.3.

Application to a simple case

We consider a chain with parameters reported in configuration 1 of Table 1. We suppose that initial deformation of the chain is defined as
$\mathbf{U}(\tau = 0) = \mathrm{u}_1(\tau = 0)\mathbf{P}_1$ and that there is no other external excitation. Therefore, $\mathbf{U}$ and $\mathbf{V}$ are expressed only using $\mathbf{P}_1$: we are able to set $\mathrm{u}_2(\tau) = 0$ and $\mathrm{v}_2(\tau) = 0$. We use the function "Eig" from Mathematica® in order to obtain exact eigenvalues and eigenvectors and we normalize the vectors of the modal base. So, we are here investigating the following case:

$$\begin{cases} L = 10 \\ \mathbf{U}(\tau) = \mathrm{u}_1(\tau)\mathbf{P}_1 \\ \mathbf{V}(\tau) = \mathrm{v}_1(\tau)\mathbf{P}_1 \\ \lambda_1 = \frac{1}{2}(3 - \sqrt{5}) \text{ first non-zero eigenvalue} \end{cases} \tag{84}$$

We obtain the following relation by injecting Eq.84 in Eq.81 and choosing $j = 1$:

$$\frac{d^2\mathrm{u}_1}{d\tau^2}(\tau) - \frac{d^2\mathrm{v}_1}{d\tau^2}(\tau) - \frac{3\Lambda}{20}\mathrm{v}_1^3(\tau) - \chi_2\frac{d\mathrm{v}_1}{d\tau}(\tau) = 0 \tag{85}$$

Noticing that we've set $L = 10$, we can see that we obtain exactly the same equation as Eq.53 during projection of the continuous system. The rest of the study will lead to the same equation of the SIM. Both continuous and discrete approaches provide similar results.

Acknowledgments

The authors would like to thank the following organizations for supporting this research: (i) The "Ministère de la transition écologique" and (ii) LABEX CELYA (ANR-10-LABX-0060) of the "Université de Lyon" within the program "Investissement d'Avenir" (ANR-11-IDEX- 0007) operated by the French National Research Agency (ANR).

Compliance with Ethical Standards:

Conflict of Interest

The authors declare that they have no conflict of interest.

References

[1] V. Veselago, "The electrodynamics of substance with simultaneously negative values of ε and ν," *Soviet Physics USPEKHI-USSR*, vol. 10, p. 509, 04 1968.

[2] G. Thompson, "Unusual waveguide characteristics associated with the apparent negative permeability obtainable in ferrites," *Nature*, vol. 175, pp. 1135–1136, 1955.

[3] K. Bertoldi, V. Vitelli, J. Christensen, and M. van Hecke, "Flexible mechanical metamaterials," *Nature Reviews*, vol. 2, p. 17066, 2017.

[4] Y. Chen, G. Hu, and G. Huang, "An adaptive metamaterial beam with hybrid shunting circuits for extremely broadband control of flexural waves," *Smart Materials and Structures*, vol. 25, p. 105036, 10 2016.

[5] L. Brillouin, *Wave Propoagation in Periodic Structures*. McGraw-Hill Book Company, Inc, 1946.

[6] X. Wang, "Dynamic behaviour of a metamaterial system with negative mass and modulus," *International Journal of Solids and Structures*, vol. 51, pp. 1534–1541, 04 2014.

[7] T.-Y. Huang, C. Shen, and Y. Jing, "Membrane- and plate-type acoustic metamaterials," *The Journal of the Acoustical Society of America*, vol. 139, no. 6, pp. 3240–3250, 2016.

[8] S. Baguet, V. Nguyen, C. Grenat, C.-H. Lamarque, and R. Dufour, "Nonlinear dynamics of micromechanical resonator arrays for mass sensing," *Nonlinear Dynamics*, vol. 95, 01 2019.

[9] L. Jezequel and C.-H. Lamarque, "Analysis of non-linear dynamical systems by the normal form theory," *Journal of Sound and Vibration*, vol. 149, pp. 429–459, 09 1991.

[10] J. Flosi, C.-H. Lamarque, and A. Ture Savadkoohi, "Periodic solutions of approximated normal forms and simplification of normal transform by using gröbner basis," *Applied Mathematical Modelling*, vol. 109, pp. 808–818, 2022.

[11] B. Lazarov and J. Thomsen, "Using high-frequency vibrations and non-linear inclusions to create metamaterials with adjustable effective properties," *International Journal of Non-linear Mechanics - INT J NON-LINEAR MECH*, vol. 44, pp. 90–97, 01 2009.

[12] O. R. Bilal, A. Foehr, and C. Daraio, "Enhancement of deep-subwavelength band gaps in flat spiral-based phononic metamaterials using the trampoline phenomena," *Journal of Applied Mechanics*, vol. 87, May 2020.

[13] H. Peng and P. Pai, "Acoustic metamaterial plates for elastic wave absorption and structural vibration suppression," *International Journal of Mechanical Sciences*, vol. 89, pp. 350–361, 12 2014.

[14] S. Mitchell, A. Pandolfi, and M. Ortiz, "Metaconcrete: Designed aggregates to enhance dynamic performance," *Journal of the Mechanics and Physics of Solids*, vol. Submitted, 01 2013.

[15] R. Zhong, Z. Zong, P. Pai, and X. Ruan, "Multi-stopband negative stiffness composite column design for vibration absorption," *Thin-Walled Structures*, vol. 144, p. 106330, 11 2019.

[16] C. da Silveira Zanin, A. Ture Savadkoohi, S. Baguet, R. Dufour, and G. Hurel, "Nonlinear vibratory energy exchanges in a meta-cell," *International Journal of Non-Linear Mechanics*, vol. 146, p. 104148, 2022.

[17] L. Cveticanin and M. Zukovic, "Negative effective mass in acoustic metamaterial with nonlinear mass-in-mass subsystems," *Communications in Nonlinear Science and Numerical Simulation*, vol. 51, pp. 89–104, 10 2017.

[18] G. S. Rodrigues and H. I. Weber, "Elastic metamaterials analysis: Simple and double resonators," 2017.

[19] L. Cveticanin, M. Zukovic, and D. Cveticanin, "Influence of nonlinear subunits on the resonance frequency band gaps of acoustic metamaterial," *Nonlinear Dynamics*, vol. 93, 08 2018.

[20] F. Romeo and G. Rega, "Wave propagation properties in oscillatory chains with cubic nonlinearities via nonlinear map approach," *Chaos Solitons & Fractals*, vol. 27, pp. 606–617, 02 2006.

[21] L. Manevitch, "The description of localized normal modes in a chain of nonlinear coupled oscillators using complex variables," *Nonlinear Dynamics*, vol. 25, pp. 95–109, 07 2001.

[22] A. Nayfeh, "Perturbation methods," 01 1973.

[23] A. Ture Savadkoohi, C.-H. Lamarque, M. Weiss, B. Vaurigaud, and S. Charlemagne, "Analysis of the 1:1 resonant energy exchanges between coupled oscillators with rheologies," *Nonlinear Dynamics*, vol. 86, pp. 2145–2159, Dec. 2016.

[24] A. Labetoulle, A. Ture Savadkoohi, and E. Gourdon, "Detection of different dynamics of two coupled oscillators including a time-dependent cubic nonlinearity," *Acta Mechanica*, vol. 233, pp. 259–290, Jan. 2022.

[25] Y. Starosvetsky and O. Gendelman, "Strongly modulated response in forced 2dof oscillatory system with essential mass and potential asymmetry," *Physica D: Nonlinear Phenomena*, vol. 237, pp. 1719–1733, 08 2008.

[26] C. Lamarque, O. Gendelman, A. Ture Savadkoohi, and E. Etcheverria, "Targeted energy transfer in mechanical systems by means of non-smooth nonlinear energy sink," *Acta Mechanica*, vol. 221, pp. 175–200, 09 2011.

[27] S. Charlemagne, C.-H. Lamarque, and A. Ture Savadkoohi, "Vibratory control of a linear system by addition of a chain of nonlinear oscillators," *Acta Mechanica*, vol. 228, 09 2017.

[28] O. Gendelman, A. Musienko, A. Vakakis, and L. Bergman, "Dynamic interaction of a semi-infinite linear chain of coupled oscillators with a strongly nonlinear end attachment," *Physica D: Nonlinear Phenomena*, vol. 178, pp. 1–18, 04 2003.

[29] B. Lazarov and J. Jensen, "Low-frequency band gaps in chains with attached non-linear oscillators," *International Journal of Non-linear Mechanics - INT J NON-LINEAR MECH*, vol. 42, pp. 1186–1193, 12 2007.

[30] A. Vakakis, M. King, and A. Pearlstein, "Forced localization in a periodic chain of non-linear oscillators," *International Journal of Non-Linear Mechanics*, vol. 29, no. 3, pp. 429–447, 1994.

[31] A. Bacigalupo, M. Lepidi, G. Gnecco, F. Vadalà, and L. Gambarotta, "Optimal design of the band structure for beam lattice metamaterials," *Frontiers in Materials*, vol. 6, p. 2, 01 2019.

[32] M.-A. Campana, M. Ouisse, E. Sadoulet-Reboul, M. Ruzzene, S. Neild, and F. Scarpa, "Impact of non-linear resonators in periodic structures using a perturbation approach," *Mechanical Systems and Signal Processing*, vol. 135, p. 106408, 01 2020.

[33] L. Wu and Y. Li, "Harnessing bulging or sloshing modes to design locally resonant liquid-solid metamaterials," *Journal of Sound and Vibration*, vol. 510, p. 116280, 06 2021.

[34] M. Barnhart, X. Xu, C. Yangyang, S. Zhang, J. Song, and G. Huang, "Experimental demonstration of a dissipative multi-resonator metamaterial for broadband elastic wave attenuation," *Journal of Sound and Vibration*, 09 2018.

[35] C. Nimmagadda and K. Matlack, "Thermally tunable band gaps in architected metamaterial structures," *Journal of Sound and Vibration*, vol. 439, 09 2018.

[36] D. Bitar, A. Ture Savadkoohi, C.-H. Lamarque, E. Gourdon, and M. Collet, "Extended complexification method to study nonlinear passive control," *Nonlinear Dynamics*, vol. 99, 01 2020.